

Chapter 1

Autoregulation of bursting of AVP neurones of the rat hypothalamus

Peter Roper¹, Colin H. Brown², Charles W. Bourque³,
and William E. Armstrong⁴

1.1 Introduction

Arginine vasopressin (AVP) is the hormone that controls both blood osmolality and pressure, and it is secreted directly into the blood by certain neurones of the neuroendocrine system. In contrast to most other CNS neurones these cells do not release neurotransmitter⁵ from their terminals at a synapse, but rather secrete AVP into the blood system, *via* exocytosis, in response to invasion of the nerve terminal by incident action potentials (spikes). In the absence of appropriate physiological stimuli, such as dehydration or a sudden drop in blood pressure, the basal secretion is low but is sufficient to maintain homeostasis. To effect this level of release the neurones emit a slow (<1.5Hz), Poisson distributed spike train. However the autonomic nervous system defends aggressively homeostasis of both blood pressure and osmolality, and a swift increase in secretion of the hormone occurs during dehydration, during haemorrhage and during carotid occlusion. Under such stimuli the cells start to fire lengthy (>20s), repeating bursts of action potentials which are separated by equally

¹Laboratory of Biological Modelling, NIDDK, Room 4007, 12A South Drive, National Institutes of Health, Bethesda, MD 20892

²School of Biomedical and Clinical Laboratory Sciences, University of Edinburgh, Edinburgh, UK

³Centre for Research in Neuroscience, Montréal General Hospital, Montréal, Canada

⁴Department of Anatomy and Neurobiology, University of Tennessee College of Medicine, Memphis, TN

⁵In fact, as in common with most neuropeptides, AVP has a dual role and can also act as a neurotransmitter, but this will not be discussed here.

lengthy silent periods [WPB78]. Mean firing rates during bursts can attain ~ 10 Hz which significantly elevates the secretion rate, while the long periods of quiescence presumably allow the cells to recover and rebuild their readily-releasable stores of the peptide. In fact these protracted bursts and silences are the most efficient mode of firing for release from AVP nerve terminals [Bic88]. There are more than 6000 AVP cells in the brain and since the entire population fires asynchronously, the total amount of peptide secreted into the blood increases smoothly with increasing stress. Phasic activity persists in *in vitro* preparations, as shown in Figure 1.1, although there do appear to be subtle differences between *in vivo* and *in vitro* activity [SBL04]. *In vitro* bursting can be evoked by either varying the osmolality of the perfusing media, or by direct depolarization [Mas80; AD83].

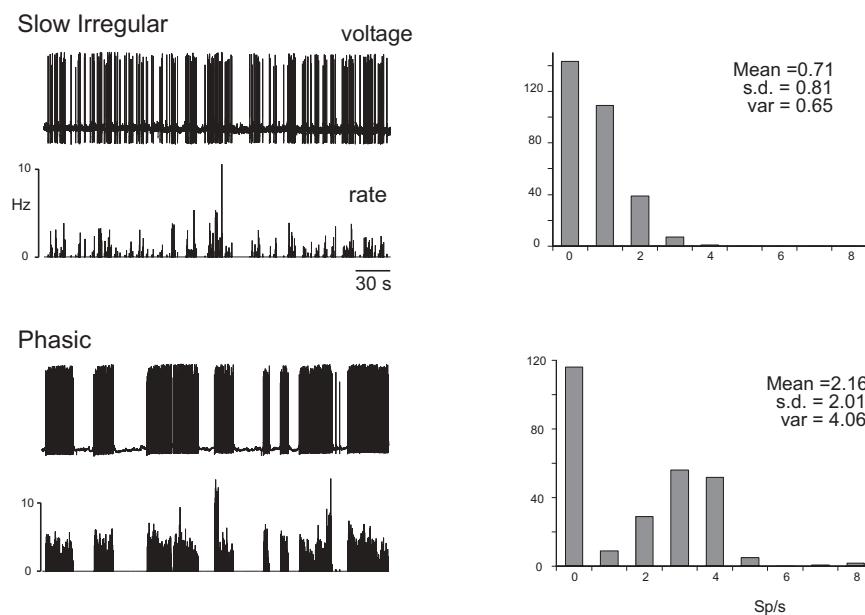


Fig. 1.1 *Slow-irregular and phasic discharge in vitro in a hypothalamic slice preparation, cf. figure 1 of [PBW88]. See [RCS⁺03; RCA04] for a description of experimental protocols. Mean firing rates are computed by averaging over a 300 second spike train divided into consecutive 1 second epochs. Slow irregular activity is the discharge pattern seen in vivo under basal conditions and is characterized by a Poissonian (variance/mean $\simeq 1$) distribution of firing rates with a skewed distribution. Phasic bursting occurs in AVP cells in vivo during times of stress, such as dehydration or haemorrhage, and is associated with a bimodal distribution of firing rates with a high (typically ~ 2.5) variance-to-mean ratio [PBW88].*

AVP is not the sole peptide released from these cells, but it is both copackaged and co-released with several other substances in the secretory vesicles, the most notable of which is the opioid peptide dynorphin. When released into the pituitary gland, dynorphin diffuses and acts on κ -opioid receptors on the terminals of neighbouring oxytocin (OT) cells to inhibit the secretion of their hormone [BGR88; SLRDMK90] by blocking calcium influx into the terminal [RGSM97], as shown in Figure 1.2. Thus dynorphin is thought to act in the neurohypophysis as a paracrine neuromodulating agent.

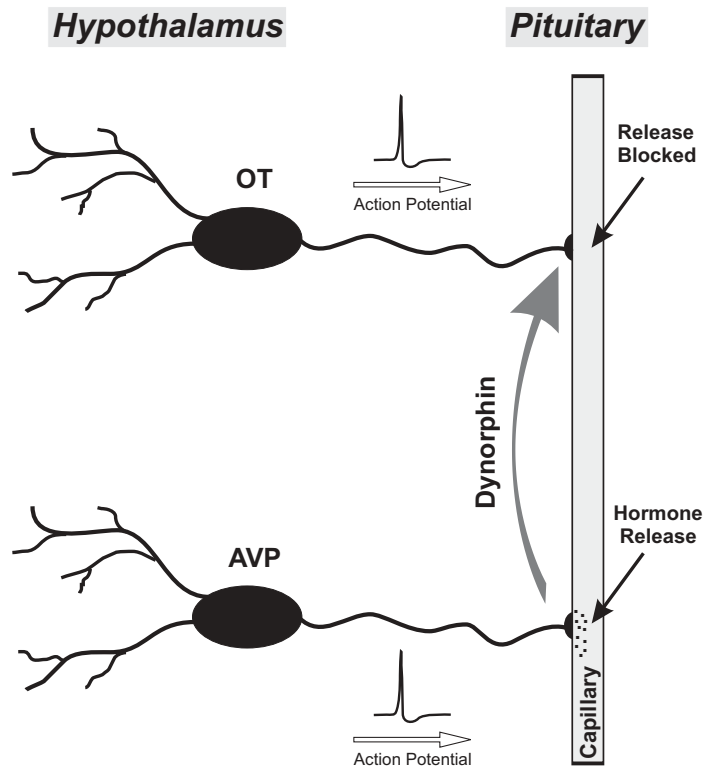


Fig. 1.2 Paracrine actions of dynorphin in the pituitary gland. The opioid peptide dynorphin is secreted from terminals of AVP cells in the neurohypophysis. It can diffuse and act via κ -opioid receptors on terminals of neighbouring oxytocin-secreting neurones to block calcium influx and so inhibit release of OT.

Release of both AVP and dynorphin occurs also within the hypothalamus *via* dense-core granule (DCG) exocytosis from the somato-dendritic region of AVP cells. However here both the range of action and the modu-

latory roles of both peptides differ from their counterparts in the neurohypophysis. AVP cells express both V_{1a} and V_2 AVP autoreceptors, and these both increase calcium influx through voltage gated channels [DSW00] when activated, and furthermore activation of the former also reduces the amplitude of incident excitatory synaptic potentials [KMHP00]. AVP diffuses widely within the nuclei before enzymatic degradation and so its release can affect both the secreting cell and also its neighbours. In contrast the diffusion of dynorphin is strongly constrained by the action of endopeptidases and so its influence is restricted to a small region around the site of secretion. Thus in the hypothalamus, AVP can be both an autocrine and a paracrine agent whilst dynorphin tends to act preferentially as an autocrine modulator. A further level of autoregulatory complexity is that the secretory vesicles also contain dynorphin sensitive κ -opioid receptors which are inserted into the cell membrane during exocytosis and thus can amplify the effects of the secreted opioid in a stimulus dependent manner [SRL+99].

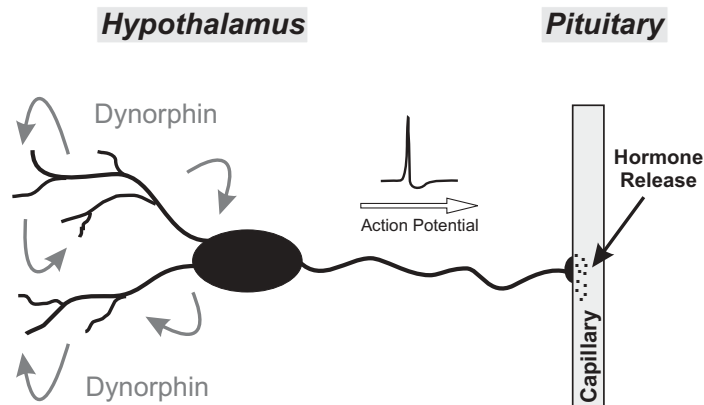


Fig. 1.3 *Autocrine actions of dynorphin in the hypothalamus. Dynorphin is released by dense-core granule exocytosis from the somato-dendritic region of AVP neurones in the hypothalamus. It acts on κ -autoreceptors on the secreting cell to modulate the cell's own electrical activity. Its diffusion is restricted by the action of endo-peptidases, and so it tends to act in an autocrine rather than a paracrine fashion.*

In this chapter we will concentrate specifically on the autocrine action of dynorphin in the supraoptic nucleus, and show how it is a key modulator of phasic bursting. Our mathematical model is based solely on *in vitro* data, but we discuss how our findings may extrapolate to *in vivo* preparations. A complete elucidation of the mathematical model can be found in [RCS+03; RCA04], and our experimental protocols are discussed fully in [RCS+03;

RCA04; BB04].

1.2 Electrical Properties of AVP cells

AVP cells *in vitro* have a resting potential close to -65mV and fire action potentials that typically reach $+40\text{mV}$ and have a half-width of $\sim 1.2\text{ms}$ [AS97]. Spike repolarization transiently overshoots rest and merges into a brief hyperpolarization, the hyperpolarizing afterpotential (HAP), which decays mono-exponentially with $\tau_{HAP} \sim 17.5\text{ms}$ and hyperpolarizes the cell by $\sim 7.4\text{mV}$ [BRR85]. A single spike briefly elevates intracellular calcium, probably *via* influx through high-voltage gated calcium channels, and the transient subsequently decays slowly. Calcium clearance after short trains of spikes follows a single exponential with time constant $\tau_{Ca} = 2.33\text{s}$ and decays toward a rest state of $C_r \equiv [\text{Ca}^{2+}]_{rest} \sim 113\text{nM}$ [RCS+03].

Single, isolated, spikes *in vitro* are succeeded by a small, lengthy transient depolarization of the membrane potential, known as the depolarizing after-potential (DAP) and shown in Figure 1.4(i)(c). The DAP is both calcium- and voltage-dependent, lasts for up to 6 seconds, raises the membrane potential by $\sim 3\text{mV}$ and its decay tracks that of $[\text{Ca}^{2+}]_i$, as shown in Figure 1.4(ii). It is thought to be caused by the temporary, calcium-mediated inhibition of a persistent potassium channel, $I_{K,leak}$, that otherwise contributes to maintenance of the resting potential (but see also [GLB02]). The DAPs that follow two or more closely spaced spikes sum to a much larger afterpotential and the resulting depolarization can take the cell above spike threshold.

Trains of evoked spikes also activate a long-lasting hyperpolarization of the membrane potential, the AHP shown in Figure 1.4b [AD84b; BRR85; AST94; KB96]. The AHP decays with a single time constant ($400 - 500\text{ms}$) [AST94; TA02], is abolished by removal of calcium, and is markedly abbreviated by apamin [BB87; AST94; KB96; Kir97], although it is not entirely abolished [GLB04]. During a train of spikes the AHP becomes manifest as a progressive increase in the inter-spike interval, and this is termed spike frequency adaptation (SFA). The AHP and the DAP overlap in time, but since the former activates more quickly than does the latter, it can overwhelm the DAP and cause an initial net hyperpolarization of the membrane. However since the AHP then decays more quickly, the more protracted DAP can appear when the AHP is attenuated.

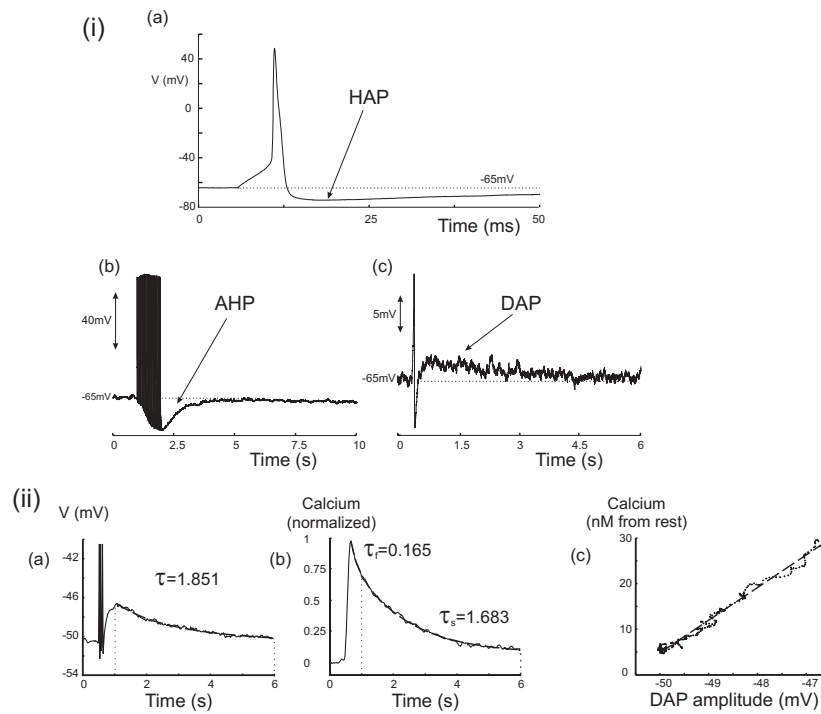


Fig. 1.4 (i) Spike after-potentials in AVP MNCs: (a) The hyperpolarizing after-potential (HAP) follows each spike and typically hyperpolarizes the cell by ~ 7.5 mV and lasts for 25–125 ms. (b) An after-hyperpolarizing potential (AHP) follows each spike train. It decays mono-exponentially with $\tau \sim 500$ ms and has a maximum amplitude ~ 12.5 mV. (c) The depolarizing after-potential (DAP) succeeds the HAP. DAPs can last for several seconds and a single DAP can depolarize the cell by ~ 3 mV. Note that the spike has been truncated for clarity. The traces are taken from whole cell (a, b) and sharp electrode (c) recordings in the slice and explant respectively. (ii) The dependency of the DAP on intracellular calcium: (a) An average of 15 DAPs from different neurones evoked with 3 spikes at 20 Hz. The baseline membrane potential was offset to be near -50 mV for all cells to reduce DAP amplitude variability and obtain a smooth decay. The decay was fit to a single exponential of 1.851, as shown by the dashed line. (b): The average somatic calcium response for the 15 DAPs. Each response was normalized to its peak. This curve was fit with a double exponential with a fast time constant of 0.165 s and a slow time constant of 1.683 s, the latter is shown by the dashed line. The vertical lines show the region of this curve (i.e. $1 \leq t \leq 6$ s) matching the DAP decay shown in the left panel. (c): The decay of the averaged DAP is plotted against the average Ca^{2+} decay. For calcium, values were converted to nM using the average peak value (41 nM) in order to appreciate the relationship between elevations in bulk calcium and the activation of the DAP. The linear fit to these responses is shown by the dashed line. Figures modified from [RCS⁺ 03].

1.3 Mathematical model

We have developed a mathematical model for the electrical activity of AVP neurones *in vitro* that is based on a set of Hodgkin-Huxley equations, and whose parameters are derived from experimental data. The full model and parameter set can be found in [RCS⁺03], but briefly it comprises a set of five currents that give rise to individual action potentials ($I_{spike} \equiv I_{Na} + I_{Ca} + I_K + I_A + I_c$), a calcium-dependent potassium AHP current I_{AHP} , and a leak current $I_{leak} = G_{leak}(V - E_{leak})$ that sets both the resting potential and the membrane time constant

$$\frac{dV}{dt} = -\frac{1}{\mathcal{C}}(I_{Na} + I_{Ca} + I_K + I_A + I_c + I_{AHP} + I_{leak} + I_{app}) \quad (1.1)$$

$$\equiv -\frac{1}{\mathcal{C}}(I_{spike} + I_{AHP} + I_{leak} + I_{app}) \quad (1.2)$$

The specific capacitance is $\mathcal{C} = 1\mu\text{F cm}^{-2}$, and I_{app} denotes the effects of any external applied current.

The active currents, (I_{spike} and I_{AHP}) have the usual Hodgkin-Huxley form (for inactivating and non-inactivating currents respectively):

$$I_\gamma = g_\gamma m^\alpha h^\beta (V - E_\gamma) \quad \text{or} \quad I_\gamma = g_\gamma m^\alpha (V - E_\gamma) \quad (1.3)$$

and their corresponding activation (*e.g.* $m(t)$) or inactivation ($h(t)$) function $x(t)$ evolves to its equilibrium state x_∞ with time constant τ_x , according to

$$\frac{d}{dt}x(t) = \frac{x_\infty - x(t)}{\tau_x} \quad (1.4)$$

Full discussion of the spiking currents can be found in [RCS⁺03] and their specifics will not be considered in detail here. If the leak current has a constant conductance ($G_{leak} = \text{const}$), then Equation (1.2) has a steady state when the applied current, I_{app} , is zero, but passes through a saddle-node bifurcation to repetitive spiking when I_{app} is increased beyond some threshold, I_{thresh} [RS02]. For $I_{app} < I_{thresh}$ the stable rest-state is excitable, and single action potentials can be elicited by transient supra-threshold stimulation. The bifurcation is characterized by a switch to repetitive firing with a frequency, ν , that increases with distance above threshold.

Equation (1.2) does not exhibit bistability (*cf.* the Morris-Lecar model presented in [RE98]) and if the bifurcation is approached from above, by reducing I_{app} below I_{thresh} , then the system reverts again to its steady state.

The neurone is considered to be isopotential and is treated as a single point, and since bulk calcium is well mixed throughout the cell it is

described by a single scalar variable, $C_i \equiv [\text{Ca}^{2+}]_i$, which obeys

$$\frac{d}{dt}C_i = -\alpha I_{Ca} - \frac{1}{\tau_{Ca}}(C_i - C_r) \quad (1.5)$$

In addition the two calcium sensitive K^+ -currents, I_c and I_{AHP} are each activated by distinct calcium microdomains, $[\text{Ca}^{2+}]_i^c$ and $[\text{Ca}^{2+}]_i^{AHP}$ respectively, which again are scalar variables and evolve independently of $[\text{Ca}^{2+}]_i$, but for simplicity their dynamics will not be considered here.

We model the current that gives rise to the apamin-sensitive AHP as a non-inactivating K^+ -current which depends solely on the calcium concentration ($C_{SK} \equiv [\text{Ca}^{2+}]_i^{AHP}$) in a small domain around the mouth of the channel

$$I_{AHP} = G_{AHP} q_\infty^2 (V - E_K) \quad (1.6)$$

where the activation, $q_\infty(C_{SK})$, is given by the Boltzman function [RCS⁺03]

$$q_\infty(C_{SK}) = \left(1 + \exp \left[-1.120 - 2.508 \log \left(\frac{C_{SK} - C_r}{1000} \right) \right] \right)^{-1} \quad (1.7)$$

We assume that the current activates instantaneously since calcium dynamics are already slow, and so the AHP decays sharply once activity has ceased, typically within 30ms of cessation of the spike train [GMRB98]. More recent evidence [GLB04] has shown that the AHP has a second, slower, apamin-insensitive component, termed the sAHP. This afterpotential is also mediated by a K^+ current, but needs many more spikes to fully activate. We have not yet incorporated this current into our model.

The DAP is modelled by dividing the leak current into separate sodium and potassium components ($I_{leak} = I_{Na,leak} + I_{K,leak}$), and while the sodium leak current is constant,

$$I_{Na,leak} = G_{Na,leak}(V - E_{Na}) \quad (1.8)$$

we let the conductance of $I_{K,leak}$ depend on both $[\text{Ca}^{2+}]_i$ and voltage according to

$$I_{K,leak} = G_{K,leak}(1 - R)(V - E_K) \quad (1.9)$$

where $G_{K,leak}$ is the maximum conductance of the current and $E_K = -90\text{mV}$ is the K^+ reversal potential.

Although $(1 - R)$ describes the modulation of a K^+ -leak conductance, it is simpler to think of R as being an activation function for the DAP. It is made up of a calcium- ($a(C_i)$) and a voltage-sensitive ($b_\infty(V)$) component

$$R(C_i, V) = \lambda - \Gamma a(C_i) b_\infty(V) \quad (1.10)$$

where λ and Γ are constants to account for the possibility that $I_{K,leak}$ can only be partially inhibited. b_∞ activates instantaneously, while a decays exponentially, with time-constant $\tau_a = 75\text{ms}$, according to Equation (1.4). a_∞ and b_∞ are given by

$$a_\infty(C_i) = \tanh\left(\frac{C_i - C_r}{k_a}\right) \quad \text{and} \quad b_\infty(V) = \left[1 + \exp\left(-\frac{V + V_b}{k_b}\right)\right]^{-1} \quad (1.11)$$

and the steady state R_∞ is shown in Figure 1.5.

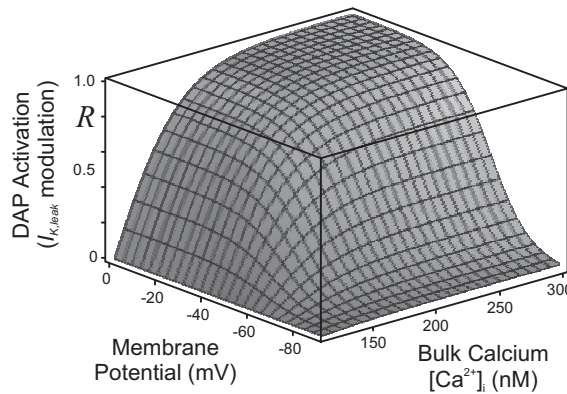


Fig. 1.5 Putative steady-state voltage- and calcium-dependent modulation of the potassium leak current, $I_{K,leak}$, or equivalently the fractional activation of the depolarizing afterpotential. See Equations (1.10) and (1.11) (reproduced from [RCS⁺ 03]).

Thus the calcium that enters the cell during an action potential increases R which partially inactivates $I_{K,leak}$ and so momentarily depolarizes the cell. After the spike, calcium starts to clear, R slowly resets and $I_{K,leak}$ returns to its rest state. This sequence of events is manifest as a transient depolarization of the membrane, and underlies the depolarizing after-potential.

Note that a_∞ , and hence so too R_∞ , can go negative if $[\text{Ca}^{2+}]_i$ is brought below rest ($C_i < C_r$), and so $I_{K,leak}$ can be both up- and down-regulated by intracellular calcium.

1.4 Firing patterns

During the basal ($\nu < 1.5\text{Hz}$) firing pattern, and in the absence of stimulation, *in vitro* cells lie subthreshold for spiking and single action potentials may be evoked when spike threshold is crossed by transient synaptic in-

put. The cells depolarize during stimulation and this progressively increases their firing rate. If the mean firing rate exceeds $\sim 1.5\text{Hz}$, then the DAPs that follow two or more closely spaced spikes can sum to a much larger afterpotential and the resulting depolarization can take the cell above spike threshold (but see also [BLL04a]), as shown in Figure 1.6(i), and this bootstrapping also occurs in the model Figure 1.6(ii). The consequent action potential then brings in more calcium, this in turn elicits another DAP which keeps the cell above threshold and the process then repeats. This spike-dependent, positive-feedback appears as a sustained plateau potential which supports repetitive spiking, and which typically persists for $\sim 20\text{s}$ before abruptly collapsing [AD83]. In the model, the DAP and the plateau potential are thus both incarnations of the inhibition of the K^+ -leak current, however to be consistent with the literature we refer to sub-threshold depolarizations as DAPs and supra-threshold potentials as plateaus.

The transition from Poisson distributed, slow-irregular firing to repeated phasic bursting can be replicated *in vitro* by direct depolarization. Furthermore, if two or three action potentials are evoked concurrently during slow-irregular firing then the resulting summed DAP can elicit a single burst, as shown in both Figure 1.6 and Figure 1.9. However such evoked bursts tend not to repeat and the cell instead returns to slow-irregular firing once the burst has ended.

1.5 Burst structure

To elucidate the mechanism that drives phasic activity we first consider the progression of a single, evoked burst in a cell that is otherwise not firing phasically. Such bursts can be triggered, both *in vivo* and *in vitro*, by antidromic stimulation; by brief spike trains triggered by short depolarizing pulses; and also by clusters of excitatory synaptic events. Although the present model includes neither synaptic input nor a mechanism for antidromic activation, current pulses can be injected by choosing a suitable protocol for the applied current, I_{app} .

Since the burst continues for many seconds beyond the end of the stimulus, it must be driven by a mechanism that is intrinsic to the cell. An example of burst initiation *in vitro* by consecutively evoked spikes is shown in the lower panel of Figure 1.6(i) and it is clear that if the summed DAP is large enough then it can steadily depolarize the cell until it crosses spike threshold and starts to fire repetitively. However if the DAP does not reach threshold then it decays and the cell returns to rest. Sub- and supra-threshold DAP summation is reproduced by the model, as shown in Figure 1.6(ii).

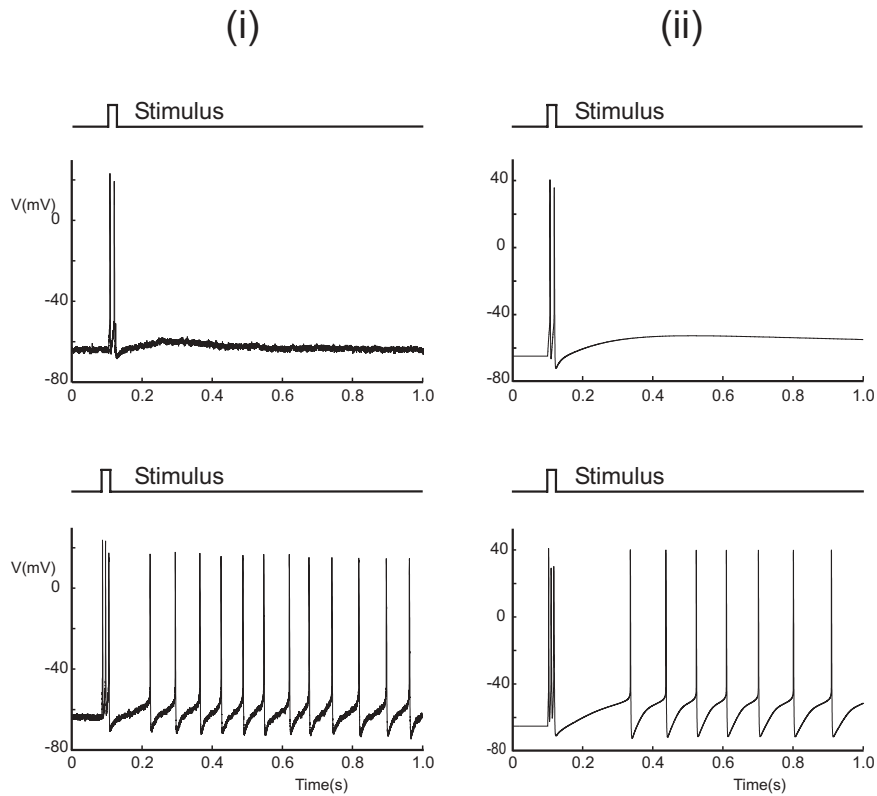


Fig. 1.6 (i) Experimental and (ii) model sub- and supra-threshold depolarizing afterpotentials (DAPs). Data taken from a whole cell recording from the SON of a hypothalamic slice, spikes evoked with a 5ms depolarizing pulse and have been truncated for clarity. Upper panels: two spikes are followed by a DAP that is sub-threshold for firing. The decay of the DAP tracks that of intracellular calcium and returns to rest with a time constant of $\tau \sim 1.85s^{-1}$ (recall Figure 1.4(i) and see [RCS⁺03]). Lower panels: DAP summation and the initiation of phasic activity: the stimulation protocol elicits three spikes and the resulting summed DAP crosses spike threshold. The consequent action potentials further raise intracellular calcium, which in turn maintains the suppression of $I_{K,leak}$ and so supports a regenerative plateau potential. This plateau then persists, and continues to support repetitive spiking, until it is inactivated by dynorphin, as discussed in Section 1.7.

The firing rate within a burst, both *in vivo* and *in vitro*, shows strong spike frequency adaptation (SFA) [PBW88; KB96], and following an initial rapid acceleration to $\sim 30\text{Hz}$ the firing gradually slows over the first couple of seconds to $\sim 10\text{Hz}$ [AD84a] and then remains steady until the end of the burst (but see section 1.7), as shown in Figure 1.7(i). The firing rate does

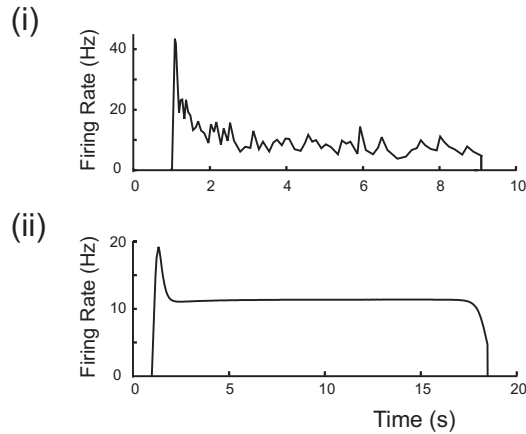


Fig. 1.7 Instantaneous firing rate (quantified by the reciprocal of the interspike interval) versus time for (i) *in vitro* experimental recording and (ii) model, cf. figure 11 of [PBW88]. Note that the rate first rises rapidly to a peak, and then slowly adapts to $\sim 10\text{Hz}$ as the apamin sensitive AHP becomes slowly activated. Firing then remains steady until the burst abruptly terminates. Figure modified from [RCA04].

decrease further during the final few spikes of the burst (see Figure 1.8), but termination is otherwise abrupt [Dyb88] and is not correlated with any further adaptation.

The initial spike-frequency adaptation can be abolished by application of 50–300nM apamin [BB87; KB96] so that the firing frequency remains high ($\sim 30\text{Hz}$) throughout the burst, and thus SFA is due to the progressive activation of the apamin sensitive AHP current (I_{AHP}) [AD84b; BB87]. Such a scenario for spike frequency adaptation also occurs in the model, as shown in the lower panel of Figure 1.7(ii). However, in contrast to the Plant model for *Aplysia* R15 [PK75], apamin block *in vitro* decreases, rather than increases, the burst length [KB96]. Furthermore the time-course of spike frequency adaptation indicates I_{AHP} is strongly activated early, rather than late, in the burst. Thus since $[\text{Ca}^{2+}]_i$ also attains its plateau early (see Section 1.6 and Figure 1.9) and does not precipitously rise during the latter stages of the burst, the primary role of I_{AHP} is likely to be the control of the firing rate within the burst and it is unlikely to contribute to burst termination.

The end of the burst is characterized by a brief slowing down of the firing rate over the final few spikes, and once spiking has ceased the plateau lingers transiently as a post-burst DAP before collapsing completely. After the active phase the cell falls quiet for another 20s or so, although it can emit occasional spikes during this time. During this silent period, the

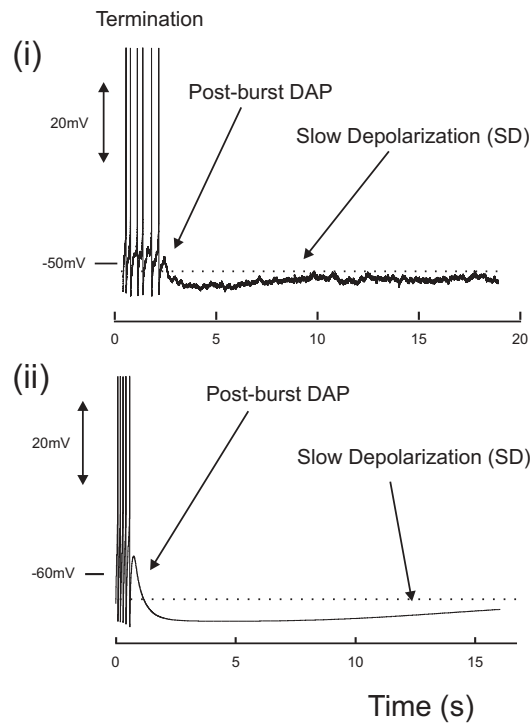


Fig. 1.8 *Burst termination and the inter-burst period: (i) whole cell electrode recording from the SON of a hypothalamic slice, and (ii) model. Note that the firing frequency remains steady until the end of the burst. The final spikes are succeeded first by a post-burst DAP, which in turn is followed by a lengthy, slow depolarization (SD). The experimental trace has been low-pass filtered to remove membrane noise and to make the general trend more evident. Spikes have been trimmed for clarity. (Reproduced from [RCA04].*

membrane potential steadily depolarizes until it comes close to, or crosses, spike threshold, and the process can then repeat. Burst termination, the transient persistence of the plateau and the subsequent slow depolarization are shown in Figure 1.8.

1.6 The role of calcium

AVP cells do not prominently express low-voltage gated calcium channels [FA96] (but see also [FB95]), and so calcium only enters the cell during an action potential, and there is no sub-threshold influx [RCS⁺03]. In consequence $[Ca^{2+}]_i$ increases only during activity and decays to its rest state

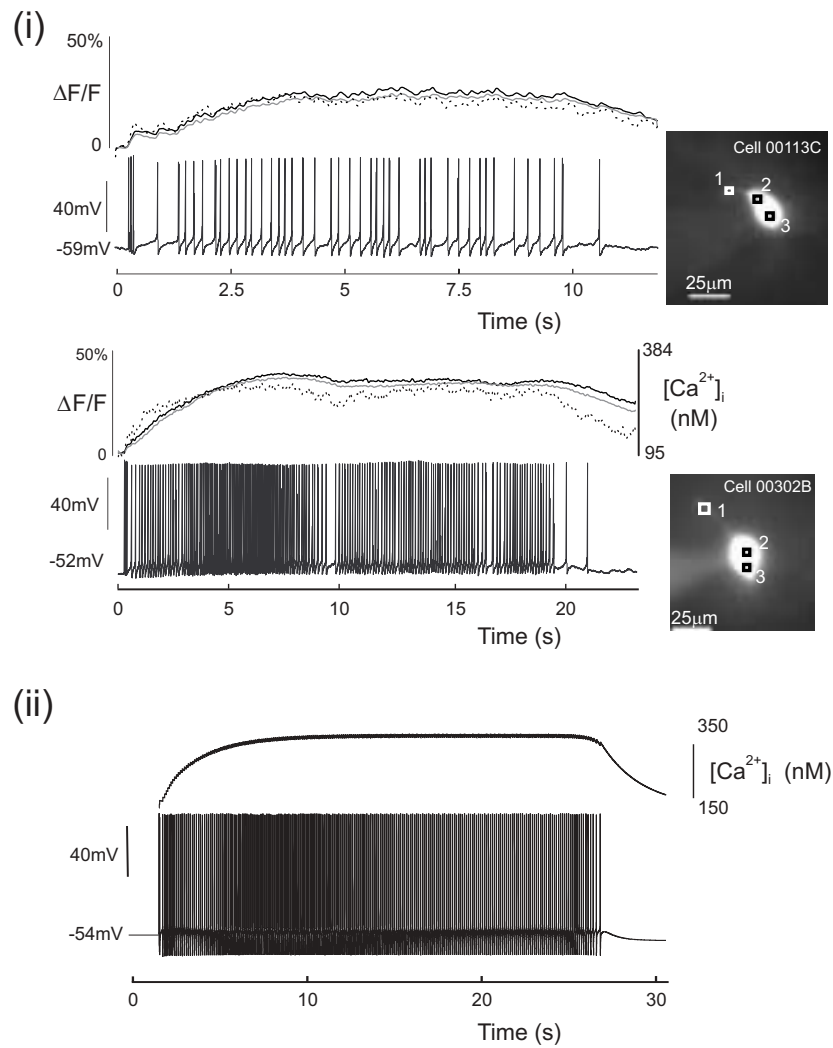
($[Ca^{2+}]_{rest} \simeq 113nM$) when the cell is silent. Figure 1.9(i) shows simultaneous whole-cell recording and calcium imaging of two evoked bursts, each of which is initiated by the summation of three DAPs. The upper trace in each figure plots the calcium concentration at three different locations in each cell. Throughout the cell $[Ca^{2+}]_i$ initially rises as the burst develops, but long before termination it reaches an elevated steady-state that is typically $>200nM$ above rest. The calcium concentration subsequently remains close to this steady-state for the remainder of the burst, and only decays when firing ceases. In the model, shown in Figure 1.9(ii), the elevated calcium plateau arises when influx is balanced by clearance, and is typically $>150nM$ supra-threshold for the full activation of the DAP. The heightened calcium concentration during the burst thus saturates the suppression of $I_{K,leak}$ and so sustains the regenerative voltage plateau for the duration of the whole active phase.

Unusually, here calcium is an agent of excitation. In other cells, *e.g.* *Aplysia* R15 bursting pacemaker cells [PK75], Ca^{2+} more typically mediates inhibition by activating a Ca^{2+} sensitive K^+ -current, whereas in AVP cells calcium excites by *inactivating* a Ca^{2+} sensitive K^+ -current.

1.7 The action of dynorphin

Dynorphin and κ -opioid receptors (for which dynorphin is the endogenous ligand) are both co-localised in AVP DCGs [SRL⁺00]. The opioid is stored in a Zn^{2+} crystalline lattice, and whilst in the granules dynorphin is prevented from binding to its receptor by a high pH. These granules are found extra-synaptically throughout the somata and dendrites of MNCs [PM89], and undergo exocytosis at the cell wall in response to Ca^{2+} influx through high-voltage-activated calcium channels [SGSM04]. Thus, somato-dendritic exocytosis of AVP is associated with electrical activity and is accompanied by high local concentrations of dynorphin over a region of cell membrane that contains newly exposed κ -opioid receptors, as shown in Figure 1.10.

When dynorphin, or its agonist, is applied exogenously *in vitro*, the amplitude of the DAP becomes reduced [BB04], as shown in Figure 1.11 and AVP cell firing is inhibited [IYY90]. In contrast κ -opioid receptor antagonists increase DAP amplitude and prolong spontaneous and evoked bursts [BB04], while oxytocin and vasopressin antagonists have no significant effect. Furthermore, since dynorphin may also activate μ -opioid receptors, as well as κ -opioid receptors, we tested a μ -opioid receptor antagonist and found no significant effect. Thus activation of κ -receptors by endogenous dynorphin must both restrain burst duration, and also cause the activity dependent reduction in DAP amplitude. Furthermore, the releasable store



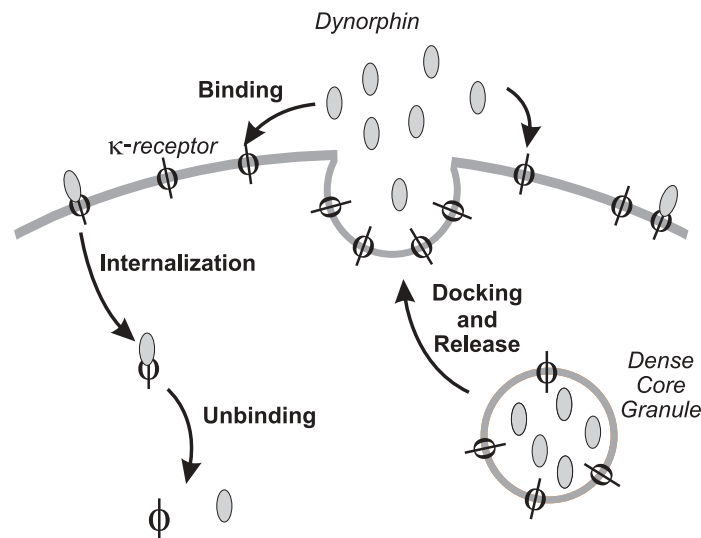


Fig. 1.10 Secretion, binding and clearance of dynorphin and κ -opioid receptors. (i) Dense-core granule (DCG) fuses to cell membrane and spills dynorphin into the extracellular space. The DCG membrane also carries κ -opioid receptors [SRL⁺99] and so fusion of the granule also upregulates the receptor. (ii) Extracellular dynorphin binds to the κ -opioid receptor, and the bound complex begins to signal. (iii) The bound complex is internalized, dephosphorylated, and ceases signalling (reproduced from [RCA04]).

of DCGs can be depleted with α -latrotoxin, and this also causes an increase in the DAP amplitude and a lengthening of burst duration. Prior application of a κ -opioid receptor antagonist prevents the inhibitory effect of α -latrotoxin on DAP amplitude [BB04], and hence endogenous dynorphin inhibition of DAPs must be mediated by DCG release.

This role of dynorphin appears to be maintained *in vivo*, and the most potent effect of κ -opioid receptor antagonists on AVP cells in anaesthetized rats is also a lengthening of burst duration [BLL98], which is similar to that which occurs *in vitro*.

κ -Opioid receptor antagonists also slightly increase AVP cell firing rate within bursts by ~ 1 Hz [BLL98]. However, this increase is not uniform across bursts; rather it is absent at the onset of the burst and emerges as each burst progresses [BLL04b]. Thus the inhibitory influence of endogenous dynorphin increases throughout the active phase in an activity dependent manner, and must be removed during the silent phase of the burst and prior to the onset of the subsequent burst. Resetting of the effect of dynorphin probably has two components: the first is that each bound dynorphin- κ -opioid receptor complex becomes internalized and de-

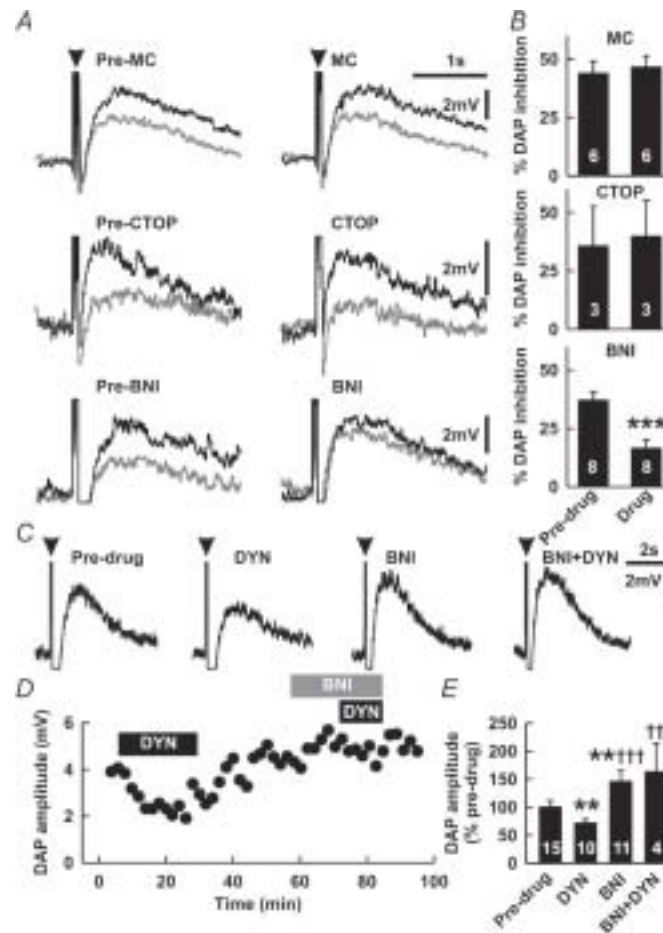


Fig. 1.11 *Endogenous κ -opioids inhibit DAPs: A, paired DAPs evoked 4 seconds before (black) and 4 seconds after (grey) a 25-spike train in the presence and absence of receptor antagonists. B, mean DAP inhibition by a 25-spike train before (Pre-drug) and during superfusion (Drug) of the AVP/oxytocin antagonist, Manning Compound (MC; 10 μ M), the μ -opioid receptor antagonist, D-Phe-Cys-Tyr-D-Trp-Orn-Thr-Pen-Thr amide (CTOP; 1 μ M), or the κ -opioid receptor antagonist, nor-binaltorphimine (BNI; 1 μ M). *** P < 0.001 versus pre-drug, paired t test. C, DAPs that each follow an 8-spike train evoked in a 12.25s cycle before and during dynorphin (1 μ M) and BNI (1 μ M) superfusion. D, time course of the opioid effects in C. E, mean DAP amplitude. ** P < 0.01 versus pre-drug and †† P < 0.01 and ††† P < 0.001 versus DYN, Student-Neuman-Keuls tests (see [BB04] for details of our statistical analysis). Reproduced from [BB04].*

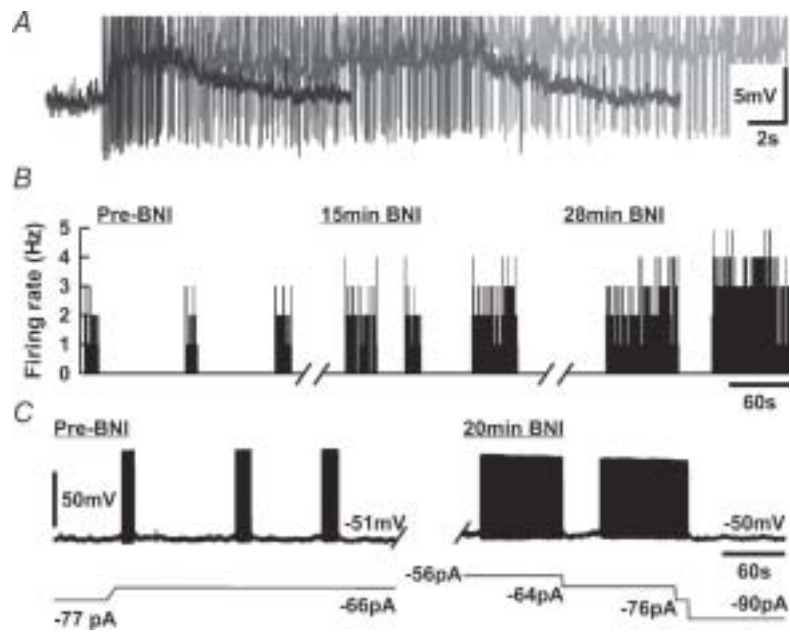


Fig. 1.12 Inhibition of autocrine κ -opioid actions prolongs spontaneous phasic bursts: A, spontaneous bursts of activity (spikes truncated) before (black) and during $1\mu\text{M}$ BNI superfusion, aligned at onset. BNI delayed plateau potential inhibition after 5 min (dark grey) and induced continuous activity after 20 min (pale grey). B, MNC spontaneous firing rate before and during BNI superfusion. BNI progressively increased the active period duration, eventually leading to continuous activity. The final period of activity shown was terminated by hyperpolarizing current injection (see C). C, membrane potential of a spontaneously phasic MNC (top trace) before (left) and during (right) superfusion of $1\mu\text{M}$ BNI. Before application of BNI, phasic activity was initiated by reducing the hyperpolarizing current injection to -66pA (bottom trace). All three Pre-BNI bursts terminated spontaneously without further manipulation of the hyperpolarizing current injection. In the presence of BNI, activity started spontaneously when the hyperpolarizing current injection was at -56pA . By contrast to activity before BNI application, in the presence of BNI activity did not spontaneously terminate; the first period of activity was terminated by increasing the hyperpolarizing current injection to -64pA . The MNC subsequently re-started firing without further adjustment of the hyperpolarizing current injection but again did not spontaneously terminate firing. Increasing the hyperpolarizing current injection to -76pA failed to terminate the second period of firing but a further increase to -90pA successfully terminated firing. Thus, during blockade of κ -opioid receptors, the MNC could spontaneously initiate activity but could not spontaneously terminate firing (as seen in 2 of 6 MNCs tested). Reproduced from [BB04].

phosphorylated, and then ceases signalling; and secondly free extracellular dynorphin is rapidly degraded by peptidases in the brain. In fact protection of endogenous dynorphin from peptidase degradation enhances the inhibition of the DAP, and so the autocrine actions of dynorphin are limited by these enzymes [BB04].

Furthermore, since the activity of adjacent AVP cells is asynchronous and dynorphin inhibition is absent at the onset of bursts, we can also infer that somato-dendritic release of dynorphin acts only in an autocrine, rather than paracrine fashion under basal conditions. It would therefore seem likely that extracellular peptidases might also act as an effective barrier to the paracrine actions of dynorphin and so inhibit synchronization of activity between AVP MNCs, and maintain a smooth secretion of the peptide, from the whole population, into the blood.

1.8 The bursting mechanism

Although dynorphin clearly plays a role in ending a burst, the actual mechanism of termination has not yet been established. It does appear that the plateau potential progressively inactivates, and that this occurs in such a way that it eventually becomes unable to sustain firing and consequently collapses [AD84b; BR91]. In addition, the successive generation of DAPs on a time-scale of several seconds significantly reduces their amplitude [BKJ98], as shown in Figure 1.13, and their subsequent recovery is slow ($\tau = 4.7\text{s}$) [BB04]. It is known that such activity-dependent inhibition can be caused by the autocrine action of dynorphin [BGLLB99], and is prevented when dynorphin antagonists are applied (see Figure 1.13), however it is still not clear how dynorphin exerts its effects on the membrane potential.

In order to keep the DAP plateau active and the cell in a repetitive firing regime, $[\text{Ca}^{2+}]_i$ needs must be maintained above the threshold for inhibiting $I_{K,leak}$. Therefore either $[\text{Ca}^{2+}]_i$ must be brought sub-threshold or the threshold must be raised for the burst to terminate. Since the calcium concentration varies little during the latter stages of the burst, see Figure 1.9, we previously inferred [RCA04] that termination is caused by an elevation of the threshold for triggering a calcium-dependent, self-sustaining plateau. We call this threshold, or separatrix, the DAP threshold and we model its desensitization by progressively decreasing the sensitivity of the DAP to calcium. We therefore propose that dynorphin acts to desensitize $I_{K,leak}$ by shifting the half-activation of R to higher calcium concentrations

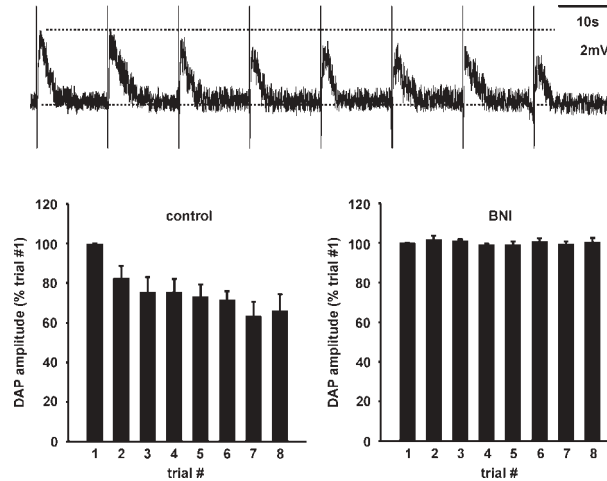


Fig. 1.13 *Top: Consecutive DAPs evoked by depolarizing current injection to elicit spike trains, each of which comprised the same number of spikes. DAPs were repeatedly evoked every 12.25 seconds and show a progressive decrease in amplitude. Bottom: Mean DAP amplitude over the course of 8 consecutive trials where DAPs were evoked 12.25s apart before (left) and during (right) BNI superfusion, showing that the progressive reduction of the DAP amplitude is caused by the endogenous activation of κ -opioid receptors.*

(see Figure 1.15). Thus Equation (1.11) becomes

$$a_{\infty}(C_i) = \tanh\left(\frac{C_i - C_r - \phi D}{k_p}\right) \quad (1.12)$$

where $\phi = 20\text{nM}$ is a scaling factor chosen to fit to data. D is a dimensionless variable that represents the indirect effect of dynorphin on the K^+ -leak current, and hence on the activation of the DAP, and as such quantifies the transduction of the bound dynorphin/ κ -opioid receptor complex. Therefore, although D is related to the extra-cellular concentration of dynorphin, the two are distinct.

We assume that D increases in some manner when the cell is active, and decreases when the cell is silent. If the half-activation shifts slowly as D increases, then $I_{K,leak}$ remains saturated and the firing rate remains steady until the DAP threshold approaches the calcium plateau. As this happens, $I_{K,leak}$ begins to reactivate, and this in turn reduces the plateau, which causes the firing rate to slow as the set of spiking currents (I_{spike}) approaches its saddle-node. Once the DAP threshold is brought above the calcium plateau, the de-sensitized DAP becomes unable to support

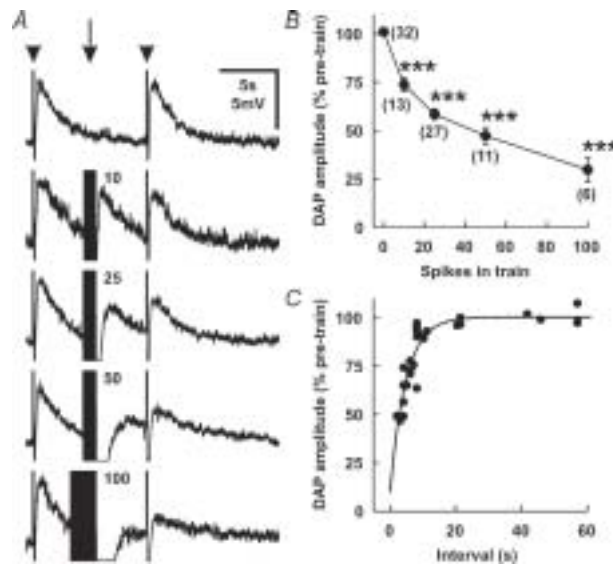


Fig. 1.14 Activity-dependent inhibition of DAPs. *A*, DAPs (averages of 5) that each follow a 5-spike train (arrowheads) evoked 9s apart by a 80ms depolarizing pulse (+150pA). A conditioning train (arrow) of 0 – 50 spikes over 1 s each, or 100 spikes over 2s, was evoked by a corresponding number of 5ms, +500pA DC pulses. *B*, DAP amplitude 4s after conditioning trains containing 0 – 100 spikes. *** $P < 0.001$ versus pre-train, Student-Newman-Keuls tests. The number of MNCs in each group is shown in parentheses. *C*, DAP amplitude at various times after a 25-spike conditioning train. A single exponential function with a time constant of 4.7s was fitted to the data ($r^2 = 0.84$, data from 9 cells). Reproduced from [BB04].

repetitive firing and so decays and firing ceases. This paradigm closely corresponds to *in vitro* activity [AD84a], and the brief persistence of the DAP is clear in the recording plotted in Figure 1.8. Although the intracellular calcium is still elevated during this time, it is now sub-threshold for DAP re-activation and, since there is no activity, there is no further influx and it decays to rest, recall Figure 1.9. *D* also decays, but if it does so more slowly than does $[Ca^{2+}]_i$, then *R* will remain shifted such that the cell stays sub-threshold and will not fire. While we do not know the true trajectory of *D*, recovery of the DAP from activity-dependent inhibition can be fit to a single exponential with time constant $\tau = 4.7s$ [BB04] (see Figure 1.14).

The model thus explains the temporal profile of the firing frequency throughout the burst. The initial rise and subsequent adaptation are caused first by the inaugural bootstrapping of the DAP summation and then by the ensuing activation of I_{AHP} . Since *R* subsequently remains saturated

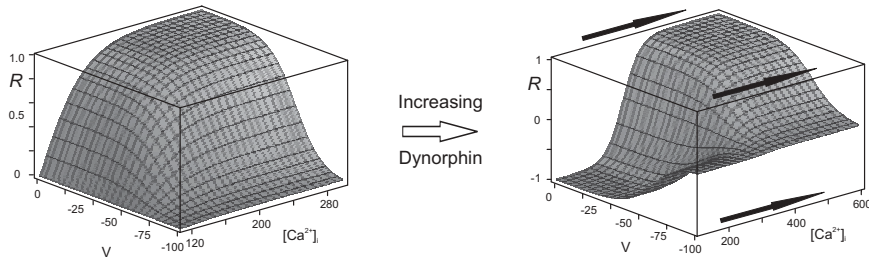


Fig. 1.15 Proposed action of dynorphin on the activation of the DAP. We suggest that the activation of the κ -opioid receptor by dynorphin desensitizes $I_{K,leak}$ to calcium and so shifts the activation curve rightward along the calcium axis. Note that the axis in the right-hand figure has been lengthened, and furthermore that for $D > 0$, R can go negative for some values of $C_i > C_r$.

($R \simeq 1$) until the end of the burst, the amplitude of the plateau, and hence the firing frequency, remains constant despite the increase in D and its attendant desensitization of $I_{K,leak}$. As the end of the burst is finally approached, R , and hence the plateau, starts to decrease until the saddle-node of I_{spike} is approached. At this time, the firing frequency starts to decrease until the saddle-node is crossed and firing ceases. Furthermore, the foreshortening of the burst by apamin [KB96] results from an increase in the activity-dependent secretion of dynorphin, and hence a more rapid increase of D due to the elevated firing rate within the burst.

A prolonged slow depolarization during the silent phase, shown in Figure 1.8(i) also arises in the model and is a consequence of $[Ca^{2+}]_i$ decaying faster than does D . Recall that our hypothesis is that dynorphin desensitizes the DAP (and thus the plateau) to calcium, thus allowing $I_{K,leak}$ to re-activate even though calcium remains elevated. The burst then terminates and both $[Ca^{2+}]_i$ and D begin to decay. However if $[Ca^{2+}]_i$ decays faster than D , it approaches its rest while D is still elevated and the calcium-dependence of the DAP is still shifted. Therefore the calcium concentration temporarily lies much lower on the $I_{K,leak}$ modulation curve than it does when the cell is at rest (recall from Equation (1.11) that a_∞ can go negative in low $[Ca^{2+}]_i$). This therefore makes R negative, and so from Equation 1.9 this in turn increases the amplitude of $I_{K,leak}$ and hyperpolarizes the cell. The hyperpolarization slowly fades as dynorphin decays and $I_{K,leak}$ eventually returns to its rest state ($R = 0$). This overshoot and slow reset is manifest as a slow depolarization of the membrane potential, and is clear in Figure 1.8(ii). The sequence of events is shown schematically in Figure 1.16.

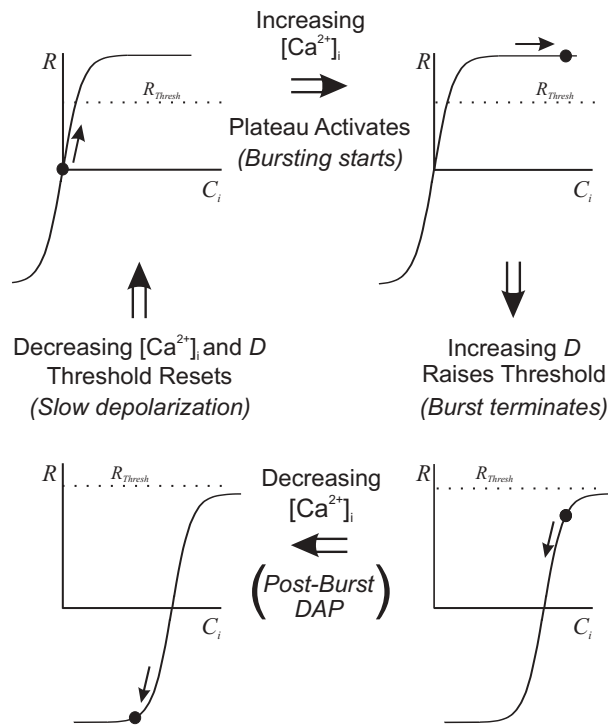


Fig. 1.16 The evolution of $[Ca^{2+}]_i$ and D throughout and between bursts, and the corresponding up- and down-modulation of $I_{K,leak}$ (shown schematically). The cycle starts from top-left and moves clockwise, and the activation of the DAP/plateau at any time is denoted by the filled circle. ‘Threshold’ denotes calcium threshold for triggering the plateau potential (not spike-threshold) and depends on spike-frequency. Note that the function R denotes the modulation (not activation) of $I_{K,leak}$ and so starts at zero, but can go negative if $[Ca^{2+}]_i$ decays while R is still right-shifted. This negative modulation corresponds to an upregulation of $I_{K,leak}$ and leads to a hyperpolarization of the membrane potential. The sequence of events is: (i) spike-driven Ca^{2+} influx depolarizes the cell by depressing $I_{K,leak}$. The depolarization triggers more spikes, further increasing $[Ca^{2+}]_i$ and so sustaining a plateau and initiating a burst; (ii) subsequent spikes cause further influx and so saturate the inhibition of $I_{K,leak}$; (iii) D starts to increase, desensitizing $I_{K,leak}$ to Ca^{2+} and raising the plateau threshold until it is no longer self-sustaining. Plateau then collapses and the burst terminates; (iv) D decays more slowly than Ca^{2+} and so remains elevated while Ca^{2+} decays. Thus $I_{K,leak}$ remains transiently desensitized, causing R to go negative and temporarily hyperpolarizing the membrane. Hyperpolarization decays as D is cleared, and becomes manifest as a slow-depolarization. As both $[Ca^{2+}]_i$ and D decay, the cell returns to its initial state. Reproduced from [RCA04].

1.9 The dynamics of dynorphin

Neuromodulation by dynorphin depends not only on its extracellular concentration, but also on the interaction between dynorphin and the κ -opioid receptor, and thus also on the κ -opioid receptor density. We assume that dynorphin is secreted from the cell's dendrites when an action potential is fired, and that it also has some clearance mechanism. To model the effects of dynorphin on the membrane potential, we represent the transduction of κ -opioid receptor activation by the dimensionless variable D which increases in some manner when the cell is active, and decreases when it is silent.

The simplest model is to assume that D is zero when the cell is at rest, is augmented by an amount Δ every time the cell spikes (or the membrane potential crosses some threshold V_{thresh}), and decreases exponentially when the cell is quiet, so that

$$\frac{d}{dt}D = -\frac{1}{\tau_D}D \quad \text{and} \quad D = D + \Delta \quad \text{when} \quad V = V_{thresh}^+ \quad (1.13)$$

where we set τ_D to be equal to the time constant for recovery from activity dependent inhibition of the DAP (*i.e.* $\tau_D = 4.7\text{s}$, see Figure 1.14), and for concreteness we set the voltage threshold $V_{thresh} = 0\text{mV}$. Whilst it appears that a single spike is able to trigger somato-dendritic secretion in oxytocin cells [dKWB⁺03], functional feedback effects of peptides thus released are only evident after clusters of spikes [BLL04b] and so Δ should be thought of as the average secretion per spike.

To include the effect of receptor insertion into the membrane, in [RCA04] we assumed that Δ depends directly on D , so that

$$\Delta(D) = \xi + \gamma D \quad (1.14)$$

where ξ is a small constant bias term that breaks the symmetry of the $D = 0$ state.

1.10 Analysis of bursting

A burst is driven by two slow variables: C_i , which is excitatory, and D , which is inhibitory and must have a slower time-course than C_i . This model differs significantly from that of [RL87] since here the slow system does not oscillate autonomously. Instead the slow variables are driven by the spiking activity since both C_i and D only increase when the cell fires an action potential.

The standard methodology for analyzing bursting models such as this one is to adiabatically decouple the full model into two disconnected subsystems [RL87], *FAST* and *SLOW*, such that:

- *FAST* includes all currents that have a time-course of milliseconds, *i.e.* those that contribute to single spikes (I_{spike})
- *SLOW* comprises all processes with a time-course of seconds, such as the calcium–dynorphin oscillation and its effect on the plateau

The AHP provides a third, distinct, time-scale ($\tau_{AHP} \simeq 500\text{ms}$). However since phasic activity still occurs during pharmacological block of I_{AHP} , and further since its major role appears to be to set the steady-state firing frequency during the burst [KB96], here we consider this current as part of the *FAST* subsystem.

1.10.1 *FAST*

The bifurcation diagram of *FAST* is shown in Figure 1.17, using the amplitude of the plateau, R as a bifurcation parameter. For $R < R_{thresh}$ *FAST* has a stable steady-state and the cell remains at rest. When R is increased above R_{thresh} , the system passes through a saddle node (SN) bifurcation to a stable limit cycle that underlies repetitive firing. The system is not bistable in the region of the SN, and so again reverts to the steady-state when R is brought back below R_{thresh} .

1.10.2 *SLOW*

The dissociation of *SLOW* from *FAST* is complicated by the fact that the two subsystems are not autonomous, and since *SLOW* is strongly coupled to *FAST* their decomposition is non-trivial. A further difficulty is that the plateau activation, R , depends not only on C_i , but also on V , which introduces a second direct coupling between *SLOW* and *FAST*. However R is saturated during most of the burst and so its voltage dependence is only effectual during the initial rise and the final fall of the plateau. Thus we may further simplify by considering only the calcium dependence.

The slow $C_i - D$ subsystem may be dissected out of the full model by using the technique of average nullclines [STR93; BRC95; BCB97], which necessitates a numerical integration of the spiking currents over the whole cycle of one action potential. However a simpler reduction can be obtained for this model by instead rewriting Equations (1.5) and (1.13) as a firing rate

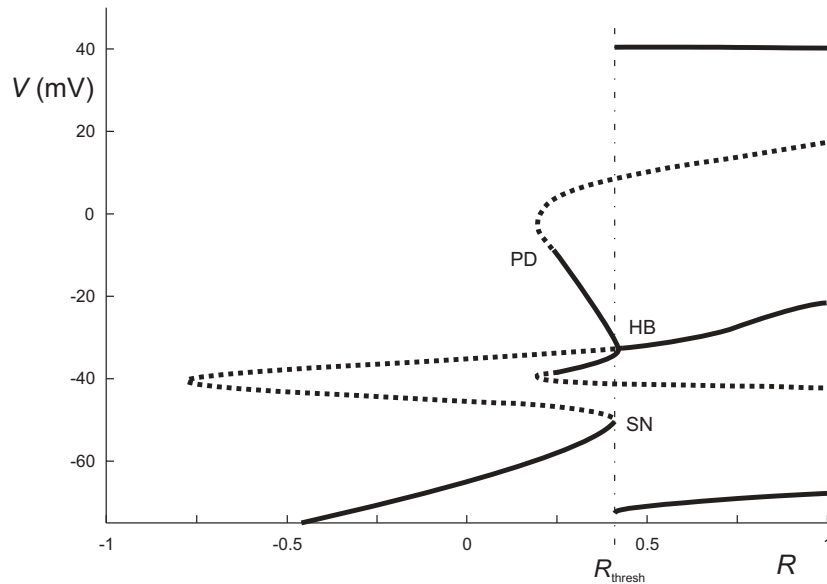


Fig. 1.17 The bifurcation diagram of FAST, for $I_{app} = 0$, using R , the relative amplitude of the plateau potential as a parameter. For $R < R_{thresh}$ FAST has a stable steady-state and the cell remains at rest. The rest state loses stability via a saddle-node bifurcation (SN) if R is raised about R_{thresh} , and FAST moves to a stable limit cycle. For larger values of R , FAST does in fact exhibit a second fixed point which bifurcates to another stable limit cycle via a Hopf bifurcation (HB), and this branch of limit cycles in turn lose stability through a period doubling (PD) bifurcation, but for $R \in [-1, 1]$ this latter manifold is not simply connected to the former by any stable trajectory. Thus it is inaccessible within the physiological range of behaviour and so does not correspond to any observed state.

model and using this *ansatz* to decouple the subsystem (see also [RL86]):

$$\frac{d}{dt}C_i = \nu(R)\Delta_{Ca} - \frac{1}{\tau_{Ca}}(C_i - C_r) \quad (1.15)$$

$$\frac{d}{dt}D = \nu(R)\Delta_D - \frac{D}{\tau_D} \quad (1.16)$$

where ν is the cell's firing frequency; Δ_{Ca} , Δ_D are the incremental increases of C_i and D per spike respectively; and $\tau_{Ca} = 2.33s$ and $\tau_D = 4.9s$ are the decay constants of calcium and D . ν is measured as the reciprocal of the time between two consecutive spikes, and is a function of the plateau activation, *viz.* $\nu \equiv \nu(R)$. In [RL86] the incremental increase of the slow variable was obtained by integrating the calcium current over a single action potential cycle, however Δ_{Ca} has been measured experimentally [RCS⁺03],

and Δ_D is not a constant, but is given by Equation (1.14).

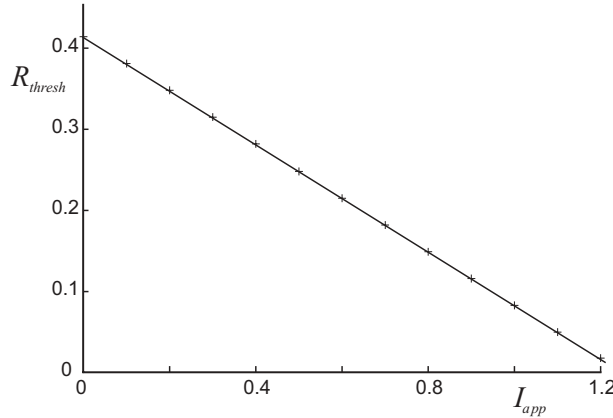


Fig. 1.18 The threshold for the activation of a regenerative plateau, R_{thresh} , depends linearly on I_{app} . Points are numerically computed values of threshold, bold line shows linear fit. Note that R_{thresh} falls below zero for $I_{app} \gtrsim 1.21$, and furthermore that since $R \equiv 0 \forall V$ when at rest (i.e. $[Ca^{2+}]_i \equiv [Ca^{2+}]_{rest}$, $D \equiv 0$), then this is the threshold for the onset of phasic activity.

We wish to examine how the dynamics of *SLOW* vary under depolarization, however the reduction given by Equations (1.15) and (1.16) does not explicitly include the effects of the applied current I_{app} . Nevertheless I_{app} does appear implicitly since its effect when increased is to raise the rest potential, and this in turn lowers the threshold for activation of the regenerative plateau, R_{thresh} . Numerically we find that R_{thresh} can be fit to a linear function of I_{app} , as shown in Figure 1.18, and so increasing I_{app} simply shifts the *FAST* bifurcation diagram (recall Figure 1.17) leftward. For large I_{app} , R_{thresh} falls below zero ($R = 0$), so that the “rest” state lies above the saddle node of the spiking currents and the cell fires continuously. However R is oscillatory during phasic activity, and so causes *SLOW* to propel *FAST* back and forth through the bifurcation. In common with the Plant model [RL86], each oscillation corresponds to a single burst/silent period. Since *FAST* is not bistable, there is no possibility for hysteresis and so *SLOW* here must comprise (at least) two slow variables, C_i and D . Furthermore the excitatory variable (C_i) must be significantly faster ($\tau_{C_a} = 2.33s$) than the inhibitory influence (D ; $\tau_D = 4.9s$) [Rin87].

The firing rate, ν , can be numerically determined for any given R , by evaluating Equation (1.2) until spike frequency adaptation is complete and then taking the reciprocal of the interspike interval. Empirically we find

that ν can be fit to the function (see Figure 1.19)

$$\nu = \begin{cases} 0 & R \leq R_{thresh} \\ \Gamma (R - R_{thresh})^\gamma & R > R_{thresh} \end{cases} \quad (1.17)$$

where both the constant, $\Gamma = 24.63$, and the exponent, $\gamma = 0.62$, are numerically determined, and we further note that since the value of R_{thresh} depends linearly on I_{app} (recall Figure 1.18) the effects of depolarization are indeed implicit, not explicit, within this system.

The nullclines of the slow system for $I_{app} = 0$ are plotted in Figure 1.20, and are similar to those of the Morris-Lecar model (see *e.g.* [ML81; RE98]): the C_i nullcline is N -shaped, while the D nullcline initially runs horizontally before increasing steeply and monotonically. (There is another symmetric nullcline for $D < 0$, but this corresponds to a non-physical solution.) The nullclines intersect at 3 fixed points, the lowest of which, $[C_i \equiv C_r, D \equiv 0]$, is stable; and small, transient, perturbations relax back to this point. However, as with the Morris-Lecar model, the system is excitable and a large excursion of *SLOW* – corresponding to an evoked burst in the full model – can be triggered if C_i is elevated by $\gtrsim 30$ nM. Such Ca^{2+} - transients typically arise *in vitro* after 2-3 concurrent spikes [RCS⁺03], and this accords with the triggering of single bursts in a non-phasic cell with a few evoked, proximal spikes (see above).

A small increase of I_{app} causes the D nullcline to shift leftward, although its shape is maintained and the fixed point remains stable. The corresponding effect on $\dot{C}_i = 0$ is twofold: the nullcline not only translates vertically, but its right-hand ‘knee’ moves further to the right. The sum of these effects that the system remains excitable but with a depressed threshold and an increased oscillation amplitude. (The increased amplitude translates to higher values of both C_i and D during the burst.) However, if I_{app} becomes large enough then the left knee of $\dot{C}_i = 0$ rises above the D nullcline, causing the two lower fixed points to coalesce and disappear in a saddle-node bifurcation. This loss of stability is the nascence of phasic activity, and examples of repetitive phasic bursting in both the model and *in vitro* are shown in Figure 1.22. Thus *SLOW* also exhibits Class I excitability: emergent, fixed-amplitude, arbitrarily low-frequency oscillations, as with the Morris-Lecar model (but *cf.* [LDL03]). Note that, in contrast to the *FAST* subsystem, each oscillation of *SLOW* represents a full burst of spikes and a subsequent silent phase, rather than a single action potential.

As I_{app} increases still further, the C_i nullcline continues to rise and the right knee moves further to the right, and so *SLOW* oscillates with a further increasing burst amplitude. Eventually the intersection of the

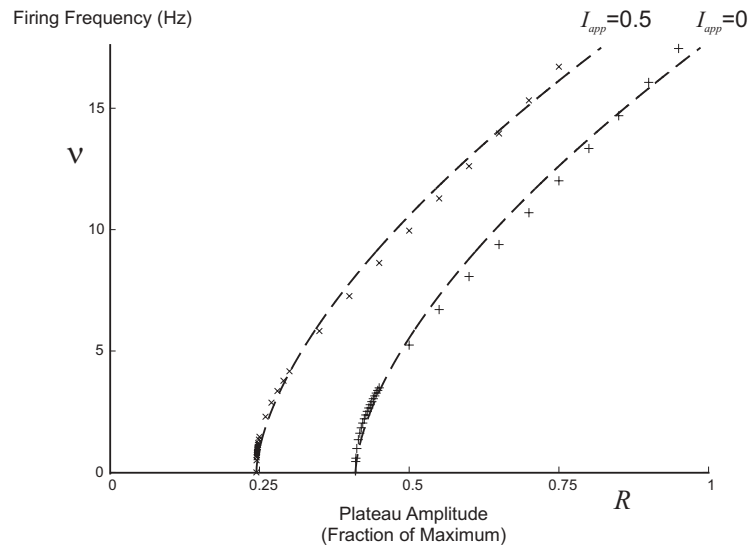


Fig. 1.19 The steady-state, intra-burst firing rate, ν , plotted as a function of R , the activation of the plateau potential, for various values of I_{app} . The intersection of $\nu(R)$ with the abscissa defines R_{thresh} for a given I_{app} , see Figure 1.18. Symbols correspond to numerically determined values of ν for different values of I_{app} : + denotes $I_{app} = 0$, while \times denotes $I_{app} = 0.5$. For any given R , $\nu(R)$ is computed by numerically evaluating Equations (1.2) and (1.9) until spike-frequency adaptation has ended and then taking the reciprocal of the interspike interval. Dashed lines show the fit to Equation (1.17). The non-linearity of $\nu(R)$ stems from the fact that R is not the amplitude of a constant depolarization, but is the modulation of a potassium current with a reversal potential.

nullclines moves from the middle branch to the left branch and so stabilizes the fixed point *via* a Hopf bifurcation. Thus *SLOW* eventually ‘locks up’ and ceases to oscillate, while *FAST* is supra-threshold, and this is the final transition from phasic to a fast-continuous pattern. Note that when the oscillation ceases, the plateau activation, R , tends to a constant, non-zero value. This is also seen *in vitro*, since a persistent plateau remains evident when fast-continuous cells are briefly hyperpolarized below spike threshold [AD84a].

SLOW therefore has three distinct modes: a subthreshold/excitabile mode, an oscillatory mode, and a steady-state that lies above spike threshold. These three modes are also enunciated on the *SLOW* subsystem bifurcation diagram plotted in Figure 1.21. The phasic behaviour seen both *in vitro* and *in vivo* may correspond not only to the oscillatory mode, but might also be engendered during the subthreshold/excitabile mode if single bursts are repeatedly evoked, *e.g.* by strong synaptic input. Finally, the

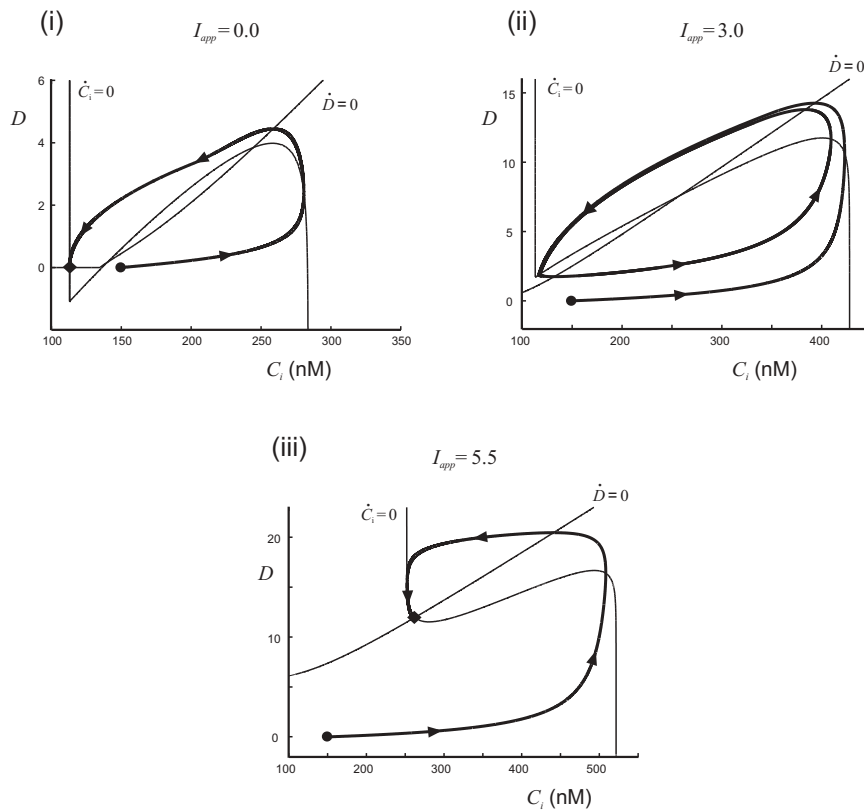


Fig. 1.20 The SLOW phase plane for increasing I_{app} . Bold lines show the trajectory of SLOW when started from an initial condition of $[C_i = 150 \text{ nM}, D = 0]$ (shown as a filled circle). This is equivalent to the calcium transient occurring after three concurrent evoked spikes. (i) $[I_{app} = 0]$ The C_i and D nullclines intersect thrice: a single, stable fixed-point $[C_i \equiv C_r, D \equiv 0]$ and two unstable fixed points. SLOW has an unstable limit cycle and is excitable for large, transient perturbations. An excitable burst is clear in the trajectory which terminates at the fixed point (filled diamond). (ii) $[I_{app} = 3.0]$ The nullclines now have only a single point of intersection. SLOW has a stable limit cycle and is therefore oscillatory, as shown in the trajectory. (iii) $[I_{app} = 5.5]$ The intersection of the C_i and D nullclines moves from the middle branch to the left branch, and SLOW stabilizes to a fixed point via a Hopf bifurcation. SLOW is still excitable when started from the initial condition $[C_i = 150 \text{ nM}, D = 0]$ but since C_r now lies above this point, the burst does not repeat.

supra spike-threshold steady state may correspond to the fast-continuous discharge mode seen during prolonged dehydration *in vivo* [PBW88].

When subthreshold, SLOW exhibits Class I excitability [Hod48; RE98] and so is directly analogous to the Morris-Lecar model for barnacle muscle

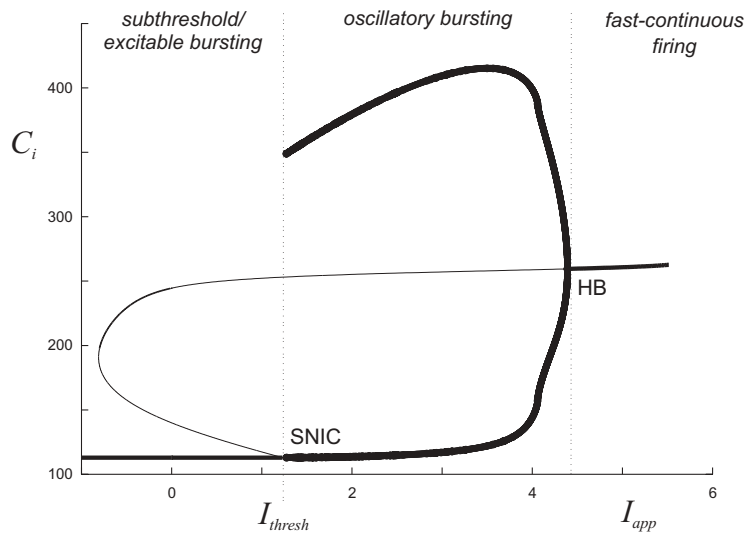


Fig. 1.21 The bifurcation diagram of the SLOW subsystem. The diagram can be subdivided into three regions, and these may be related to the three modes of behaviour observed both in vitro and in vivo. The left-hand section of the diagram has a only a single stable fixed point, which is below spike-threshold and corresponds to the resting state. In this region SLOW is excitable and a single burst can be evoked when C_i is transiently elevated. When I_{app} is raised above I_{thresh} , the stable fixed point collides with an unstable fixed point and they coalesce in a saddle-node bifurcation (SNIC). Thus the center of the diagram contains a stable limit cycle, which corresponds to repetitive, phasic bursting. As I_{app} increases yet further, the limit cycle disappears in a Hopf bifurcation (HB) so that the right-hand side of the diagram again has only a single, stable fixed-point. However, this fixed point is now supra-threshold for spiking, and so this mode may correspond to the fast continuous spiking seen during sustained dehydration in vivo.

fibres [ML81]. Excitable bursting of this sort was discussed briefly by [Izh00] (but see also [SSP95; BCB97]), and was analyzed extensively, within the context of the ghost-burster model [DLLM02] for the pyramidal cells of weakly electric fish, by [LDL03]. However the reduction presented here is closer in spirit to the Morris-Lecar model than is the ghost-burster, since the latter is only excitable when the corresponding FAST subsystem is oscillating periodically. The ghost-burster's excitability therefore depends on the phase of FAST at the time of stimulation, while our AVP model shows no phase dependence, and so here the analogy with type I excitability is exact.

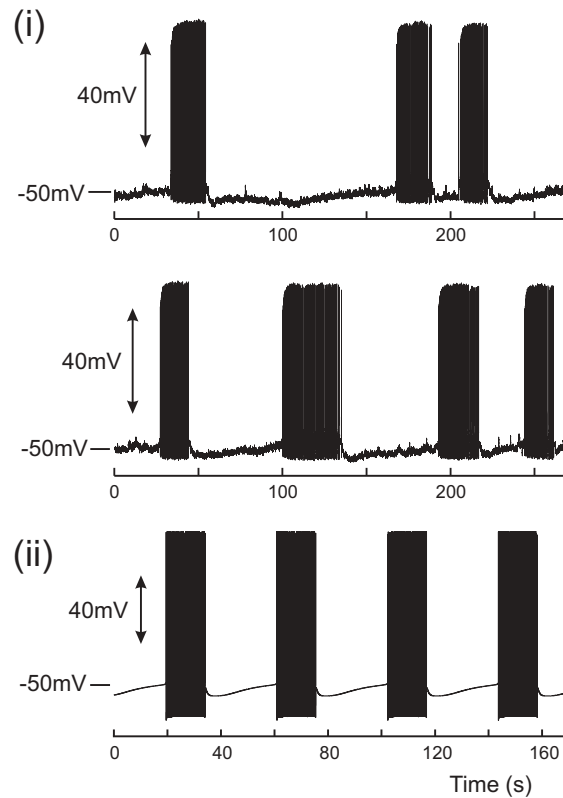


Fig. 1.22 Phasic activity occurring in MNC's during sustained depolarization: (i) experimental recordings and (ii) model. Note silent phase characterized first by post-burst DAP, and then by slow depolarization. Both active and silent phases of the burst have mean length ~ 20 s (see text), but display a wide variability both in vitro and in vivo. Model parameters are $I_{app} = 1.28$, $\lambda = 0.6$ and $\Gamma = 0.4$. Phasic activity only occurs when the model is depolarized above spike-threshold, and the oscillation is driven by an upregulation of $I_{K,leak}$ which transiently depresses V below threshold and interrupts firing. Reproduced from [RCA04].

1.11 Discussion

1.11.1 A dual role for calcium

By activating the AHP, calcium is usually perceived as a messenger of electrical inhibition rather than excitation (see *e.g.* [VLMA98]). However in AVP cells it plays two opposing roles: not only does it mediate both short- and long-term inhibition *via* the activation of BK and SK channels (I_c and

I_{AHP}), but it can also excite the cell by turning off the resting K^+ current, $I_{K,leak}$ [LH97]. Having two such antithetical functions appears at first glance to be contradictory. However there is a delicate interplay between the DAP and the AHP that is dictated by their respective time-scales, and whether the cell exhibits a depolarizing or a hyperpolarizing after-potential depends both on the stimulation frequency and also the number of spikes in the train [AD84b]. In phasic neurones strongly expressing DAPs, prolonged low frequency stimulation ($<1\text{Hz}$) evokes single spikes and consequent DAPs, which then fade to the resting potential. At intermediate frequencies ($>1\text{Hz}$ and $<10\text{Hz}$) the DAPs sum to form a regenerative depolarized plateau potential which can then support endogenous firing *via* positive feedback [AD83]. In contrast, at higher frequencies ($>10\text{Hz}$) the AHP becomes predominant and instead a net hyperpolarization occurs (see Figure 1.4b). Thus calcium acts here both to amplify signals of a certain bandwidth, and to filter stimulation that is of too high or too low a frequency. Furthermore, since the DAP is also voltage-dependent, this signal processing is labile and depends on the membrane potential. Thus the depolarization occurring during osmotic stress magnifies the gain of the amplification, and contributes to phasic activity.

1.11.2 *Alternative mechanisms for the plateau potential*

Here we have adopted the paradigm, initially proposed by [LH97], that the DAP is a Ca^{2+} -mediated reduction in a resting K^+ -current. Not only does this model show burst initiation and termination profiles that closely agree with experiment, but it also clarifies some more subtle features of the cells' electrical activity (*e.g.* the post-burst DAP and the intra-burst slow-depolarization). However, it is also possible that DAP is caused by a Ca^{2+} -activated non-specific cation (CAN) current [Bou86; GLB02].

In [RCA04] we also examined a model based on the activation and modulation of a CAN current, and showed that, to a first approximation, both models are equivalent since the former is the addition of a depolarizing current while the latter is the subtraction of a hyperpolarizing current. If we also assume that desensitization to Ca^{2+} causes burst termination in both cases, then both models support burst initiation, the plateau potential and burst termination, and so their active phases are indistinguishable. However, recall that R goes negative when $[\text{Ca}^{2+}]_i < [\text{Ca}^{2+}]_{rest}$ and that this causes the slow-depolarization between bursts. In our model this can be readily interpreted as an upregulation of the resting current $I_{K,leak}$, but if $I_{CAN} = 0$ at rest in the CAN model, then the corresponding mechanism is less fathomable since it should not reverse in low calcium.

We therefore proposed that if I_{CAN} were to be a persistent current,

contributing to the resting membrane potential in a similar manner to that which we originally proposed for $I_{K,leak}$, then it is conceivable that it too could be both up- and down-regulated by $[Ca^{2+}]_i$ and dynorphin. Thus a CAN model can only fully explain phasic activity if it is driven by a non-specific cation current that is partially active at rest. Such a current has recently been observed by [HGSK03], but it has not yet been shown to be modulated by $[Ca^{2+}]_i$.

1.11.3 *Excitable bursting*

Is burst excitability physiologically useful, or is it merely an artefact of the dynamics? The answer probably lies in the ability of these nuclei to respond to and to integrate multifarious inputs. Recall that phasic firing is the discharge mode most efficient for release from AVP nerve terminals [Bic88]. Thus, while some efferents, *e.g.* histaminergic inputs from the tuberomammillary nucleus [AS85; LH96], cause a tonic and sustained depolarization and so might induce oscillatory, or supra-threshold bursting. Others, for example NMDA receptor activation [MMGH94], have a punctuate effect on the cells membrane potential and so can only elicit single spikes. Nevertheless, such discrete input can evince a phasic discharge if excitable bursts are repeatedly evoked, and this may in turn be achieved by triggering spikes with a mean rate of as low as 3Hz [PBW88]. Thus for MNCs *in vivo*, excitable bursting might allow the SON swiftly to amplify intermittent synaptic input into the most efficient discharge mode for secretion.

Acknowledgements

We thank Chunyun (Lisa) Li (University of Tennessee, Memphis) and Ry-
oichi Teruyama (University of Tennessee, Memphis) for allowing us to re-
produce their data, shown in Figure 1.1, and Figures 1.4, 1.6, 1.7, 1.8 and
1.22 respectively. We also thank Bard Ermentrout (University of Pitts-
burgh) for releasing, and supporting XPPaut⁶, which was used for all of
our numerical work. We also thank Arthur Sherman (NIDDK) both for
support and guidance during this work, and for a careful critique of this
chapter.

PR and CHB are supported by fellowships from NIH/NIDDK and Wel-
come respectively; WEA is supported by NIH grant number NS23941; and
CWB is supported by Operating and Senior Investigator Awards from the
Canadian Institutes of Health Research, and by a James McGill Research
Chair.

⁶<http://www.math.pitt.edu/~bard/xpp/xpp.html>

Bibliography

- R.D. Andrew and F.E. Dudek. Burst discharge in mammalian neuroendocrine cells involves an intrinsic regenerative mechanism. *Science*, 221(4615):1050–1052, 1983.
- R.D. Andrew and F.E. Dudek. Analysis of intracellularly recorded phasic bursting by mammalian neuroendocrine cells. *Journal of Neurophysiology*, 51(3):552–566, 1984.
- R.D. Andrew and F.E. Dudek. Intrinsic inhibition in magnocellular neuroendocrine cells of rat hypothalamus. *Journal of Physiology (London)*, 353:171–185, 1984.
- W.E. Armstrong and C.D. Sladek. Evidence for excitatory actions of histamine on supraoptic neurons *in vitro*: Mediation by an H₁-type receptor. *Neuroscience*, 16:307–322, 1985.
- W.E. Armstrong and J.E. Stern. Electrophysiological and morphological characteristics of neurons in perinuclear zone of supraoptic nucleus. *Journal of Neurophysiology*, 78(5):2427–2437, 1997.
- W.E. Armstrong, B.N. Smith, and M. Tian. Electrophysiological characteristics of immunohistochemically identified rat oxytocin and vasopressin neurons *in vitro*. *Journal of Physiology (London)*, 475(1):115–128, 1994.
- C.W. Bourque and D.A. Brown. Apamin and d-tubocurarine block the after-hyperpolarization of rat supraoptic neurosecretory neurons. *Neuroscience Letters*, 82(2):185–190, 1987.
- C.H. Brown and C.W. Bourque. Autocrine feedback inhibition of plateau potentials terminates phasic bursts in magnocellular neurosecretory cells of the rat supraoptic nucleus. *Journal of Physiology (London)*, 557(3):949–960, 2004.
- R.J. Butera, Jr., J.W. Clark, Jr., and J.H. Byrne. Transient responses of a modeled bursting neuron: analysis with equilibrium and averaged nullclines. *Biological Cybernetics*, 77(5):307–322, 1997.
- C.H. Brown, M. Ghamari-Langroudi, G. Leng, and C.W. Bourque. κ -opioid receptor activation inhibits post-spike depolarizing after-potentials in rat supraoptic nucleus neurons *in vitro*. *Journal of Neuroendocrinology*, 11(11):825–828, 1999.

- C.A. Bondy, H. Gainer, and J.T. Russell. Dynorphin A inhibits and naloxone increases the electrically stimulated release of oxytocin but not vasopressin from the terminals of the neural lobe. *Endocrinology*, 122(4):1321–1327, 1988.
- R.J. Bicknell. Optimizing release from peptide hormone secretory nerve terminals. *Journal of Experimental Biology*, 139:51–65, September 1988.
- C.W. Bourque, K. Kirkpatrick, and C.R. Jarvis. Extrinsic modulation of spike afterpotentials in rat hypothalamoneurohypophysial neurons. *Cellular and Molecular Neurobiology*, 18(1):3–12, 1998.
- C.H. Brown, M. Ludwig, and G. Leng. κ -opioid regulation of neuronal activity in the rat supraoptic nucleus *in vivo*. *Journal of Neuroscience*, 18(22):9480–9488, 1998.
- C.H. Brown, M. Ludwig, and G. Leng. Phasic bursts in rat magnocellular neurosecretory cells are not intrinsically regenerative *in vivo*. *European Journal of Neuroscience*, 19(11):2977–2983, 2004.
- C.H. Brown, M. Ludwig, and G. Leng. Temporal dissociation of the feedback effects of dendritically co-released peptides on rhythmogenesis in vasopressin cells. *Neuroscience*, 124(1):105–111, 2004.
- C.W. Bourque. Calcium-dependent spike after-current induces burst firing in magnocellular neurosecretory-cells. *Neuroscience Letters*, 70(2):204–209, 1986.
- C.W. Bourque and L.P. Renaud. Membrane-properties of rat magnocellular neuroendocrine cells *in vivo*. *Brain Research*, 540(1-2):349–352, 1991.
- S.M. Baer, J. Rinzel, and H. Carrillo. Analysis of an autonomous phase model for neuronal parabolic bursting. *Journal of Mathematical Biology*, 33:309–333, 1995.
- C.W. Bourque, J.C.R. Randle, and L.P. Renaud. Calcium-dependent potassium conductance in rat supraoptic nucleus neurosecretory neurons. *Journal of Neurophysiology*, 54(6):1375–1382, 1985.
- C.P. de Kock, K.D. Wierda, L.W. Bosman, R. Min, J.J. Kokksma, H.D. Mansvelter, M. Verhage, and A.B. Brussaard. Somatodendritic secretion in oxytocin neurons is upregulated during the female reproductive cycle. *Journal of Neuroscience*, 23(7):2726–34, May 2003.
- B. Doiron, C. Laing, A. Longtin, and L. Maler. Ghostbursting: a novel neuronal burst mechanism. *Journal of Computational Neuroscience*, 12:5–25, 2002.
- G. Dayanithi, N. Sabatier, and H. Widmer. Intracellular calcium signalling in magnocellular neurones of the rat supraoptic nucleus: understanding the autoregulatory mechanisms. *Experimental Physiology*, 85(SISI):S75–S84, 2000.
- R.E.J. Dyball. The importance of bursting in determining secretory responses: How does a phasic firing pattern influence peptide release from neurohypophyseal vasopressin terminals. In G. Leng, editor, *Pulsatility in Neuroendocrine Systems*, chapter 10, pages 181–196. CRC Press, Inc, Boca Raton, Florida, 1988.
- R.C. Foehring and W.E. Armstrong. Pharmacological dissection of high-voltage-activated Ca^{2+} current types in acutely dissociated rat supraoptic magno-

- cellular neurons. *Journal of Neurophysiology*, 76(2):977–983, 1996.
- T.E. Fisher and C.W. Bourque. Voltage-gated calcium currents in the magnocellular neurosecretory cells of the rat supraoptic nucleus. *Journal of Physiology (London)*, 486(3):571–580, 1995.
- M. Ghamari-Langroudi and C.W. Bourque. Flufenamic acid blocks depolarizing afterpotentials and phasic firing in rat supraoptic neurones. *Journal of Physiology (London)*, 545(2):537–542, 2002.
- M. Ghamari-Langroudi and C. W. Bourque. Muscarinic receptor modulation of slow afterhyperpolarization and phasic firing in rat supraoptic nucleus neurons. *Journal of Neuroscience*, 24(35):7718–7726, September 2004.
- W. Greffrath, E. Martin, S. Reuss, and G. Boehmer. Components of afterhyperpolarization in magnocellular neurons of the rat supraoptic nucleus *in vitro*. *Journal of Physiology (London)*, 513(2):493–506, 1998.
- J. Han, C. Gnatenco, C.D. Sladek, and D. Kim. Background and tandem-pore potassium channels in magnocellular neurosecretory cells of the rat supraoptic nucleus. *Journal of Physiology*, 546:625–639, 2003.
- A.L. Hodgkin. The local electric changes associated with repetitive action in a non-medullated axon. *Journal of Physiology (London)*, 107:165–181, 1948.
- K. Inenaga, H. Imura, N. Yanaihara, and H. Yamashita. κ -selective opioid receptor agonists leuorphan and dynorphin inhibit supraoptic neurons in rat hypothalamic slice preparations. *Journal of Neuroendocrinology*, 2:389–396, 1990.
- E.M. Izhikevich. Neural excitability, spiking, and bursting. *International Journal of Bifurcation and Chaos*, 10(6):1171–1266, 2000.
- K. Kirkpatrick and C.W. Bourque. Activity dependence and functional role of the apamin-sensitive K^+ current in rat supraoptic neurones *in vitro*. *Journal of Physiology (London)*, 494(2):389–398, 1996.
- K. Kirkpatrick. *Functional role and modulation of a calcium-activated potassium current in rat supraoptic neurons in vitro*. PhD thesis, Department of Neurology and Neurosurgery, McGill University, Montreal, 1997.
- S.B. Kombian, D. Mouginot, M. Hirasawa, and Q.J. Pittman. Vasopressin preferentially depresses excitatory over inhibitory synaptic transmission in the rat supraoptic nucleus *in vitro*. *Journal of Neuroendocrinology*, 12(4):361–367, 2000.
- C. Laing, B. Doiron, and A. Longtin. Type I burst excitability. *Journal of Computational Neuroscience*, 14(3):329–342, 2003.
- Z. Li and G.I. Hatton. Histamine-induced prolonged depolarization in rat supraoptic neurons: G-protein-mediated, Ca^{2+} -independent suppression of k^+ leakage conductance. *Neuroscience*, 70(1):145–158, 1996.
- Z.H. Li and G.I. Hatton. Reduced outward K^+ conductances generate depolarizing after-potentials in rat supraoptic nucleus neurones. *Journal of Physiology (London)*, 505(1):95–106, 1997.
- W.T. Mason. Supraoptic neurones of rat hypothalamus are osmosensitive. *Nature*, 287(11):154–157, September 1980.
- C. Morris and H. Lecar. Voltage oscillations in the barnacle giant muscle fiber. *Biophysical Journal*, 35(1):193–213, July 1981.

- R.B. Meeker, S. McGinnis, R.S. Greenwood, and J.N. Hayward. Increased hypothalamic glutamate receptors induced by water deprivation. *Neuroendocrinology*, 60(5):477–485, 1994.
- D.A. Poulain, D. Brown, and J.B. Wakerley. Statistical analysis of patterns of electrical activity in vasopressin- and oxytocin-secreting neurones. In G. Leng, editor, *Pulsatility in Neuroendocrine Systems*, chapter 8, pages 119–154. CRC Press, Inc, Boca Raton, Florida, 1988.
- R.E. Plant and M. Kim. On the mechanism underlying bursting in the Aplysia abdominal ganglion R15 cell. *Mathematical Biosciences*, 26:357–375, 1975.
- D.V. Pow and J.F. Morris. Dendrites of hypothalamic magnocellular neurons release neurohypophysial peptides by exocytosis. *Neuroscience*, 32(2):435–439, 1989.
- P. Roper, J. Callaway, and W. Armstrong. Burst initiation and termination in phasic vasopressin cells of the rat SON. *Journal of Neuroscience*, 24(20):4818–4831, 2004.
- P. Roper, J. Callaway, T. Shevchenko, R. Teruyama, and W. Armstrong. AHP's, HAP's and DAP's: How potassium currents regulate the excitability of rat supraoptic neurones. *Journal of Computational Neuroscience*, 15(3):367–389, 2003.
- J. Rinzel and B. Ermentrout. Analysis of neural excitability and oscillations. In C. Koch and I. Segev, editors, *Methods in Neuronal Modeling: From Ions to Networks*, chapter 7, pages 251–291. MIT Press, Inc, Cambridge, Massachusetts, 2nd edition, 1998.
- K.I. Rusin, D.R. Giovannucci, E.L. Stenkel, and H.C. Moises. κ -receptor activation modulates currents and secretion in isolated neuroendocrine nerve terminals. *Journal of Neuroscience*, 17(17):6565–6574, 1997.
- J. Rinzel. A formal classification of bursting mechanisms in excitable systems. In E. Teramoto and M. Yamaguti, editors, *Mathematical Topics in Population Biology, Morphogenesis and Neurosciences*, number 71 in Lecture Notes in Biomathematics, pages 267–281. Springer-Verlag, 1987.
- J. Rinzel and Y. S Lee. On different mechanisms for membrane potential bursting. In H.G. Othmer, editor, *Nonlinear Oscillations in Biology and Chemistry*, number 66 in Lecture Notes in Biomathematics, pages 19–33. Springer-Verlag, 1986.
- J. Rinzel and Y.S. Lee. Dissection of a model for neuronal parabolic bursting. *Journal of Mathematical Biology*, 25:653–675, 1987.
- P. Roper and A. Sherman. Mathematical analysis of firing pattern transitions in rat SON magnocellular neurosecretory cells subject to osmotic stress. *Society for Neuroscience Abstracts*, 28(273.3), 2002.
- N. Sabatier, C.H. Brown, M. Ludwig, and G. Leng. Phasic spike patterning in rat supraoptic neurones *in vivo* and *in vitro*. *Journal of Physiology (London)*, 558:161–180, 2004.
- B.L. Soldo, D.R. Giovannucci, E.L. Stuenkel, and H.C. Moises. Ca^{2+} and frequency dependence of exocytosis in isolated somata of magnocellular supraoptic neurones of the rat hypothalamus. *Journal of Physiology (London)*, 555(Pt 3):699–711, March 2004.

Bibliography

39

- J.Y. Summy-Long, L.M. Rosella-Dampman, G.L. McLemore, and E. Koehler. Kappa opiate receptors inhibit release of oxytocin from the magnocellular system during dehydration. *Neuroendocrinology*, 51(4):376–84, April 1990.
- S.J. Shuster, M. Riedl, X. Li, L. Vulchanova, and R. Elde. Stimulus-dependent translocation of κ opioid receptors to the plasma membrane. *Journal of Neuroscience*, 19(7):2658–2664, 1999.
- S.J. Shuster, M. Riedl, X. Li, L. Vulchanova, and R. Elde. The κ opioid receptor and dynorphin co-localize in vasopressin magnocellular neurosecretory neurons in guinea-pig hypothalamus. *Neuroscience*, 96(2):373–383, 2000.
- E. Sivan, L. Segel, and H. Parnas. Modulated excitability: a new way to obtain bursting neurons. *Biological Cybernetics*, 72(5):455–461, 1995.
- P. Smolen, D. Terman, and J. Rinzel. Properties of a bursting model with two slow inhibitory variables. *SIAM Journal on Applied Mathematics*, 53(3):861–892, 1993.
- R. Teruyama and W.E. Armstrong. Changes in the active membrane properties of rat supraoptic neurons during pregnancy and lactation. *Journal of Neuroendocrinology*, 14:1–17, 2002.
- C. Vergara, R. Latorre, N.V. Marrion, and J.P. Adelman. Calcium-activated potassium channels. *Current Opinion in Neurobiology*, 8(3):321–329, 1998.
- J.B. Wakerley, D.A. Poulain, and D. Brown. Comparison of firing patterns in oxytocin- and vasopressin-releasing neurones during progressive dehydration. *Brain Research*, 148:425–440, 1978.